Computational Studies on Bimetallic Clusters

DISSERTATION FOR THE DEGREE OF DOCTOR PHILOSOPHIAE

Ying-Chan Lin
Laboratory for Instruction in Swedish
Department of Chemistry
University of Helsinki
Helsinki, Finland

To be presented, with permission of the Faculty of Science, University of Helsinki, for public discussion in Auditorium A129, Department of Chemistry (A.I. Virtanens plats 1, Helsinki), June the 27th, 2008, at 10 o'clock.

Helsinki 2008

Supervised by

Doc. Dage Sundholm
Department of Chemistry
University of Helsinki

Revised by

Dr. Nino Runeberg
CSC

Doc. Perttu Lantto
Academy of Finland

ISBN 978-952-10-4746-6 (paperback)
ISBN 978-952-10-4747-3 (PDF)
http://ethesis.helsinki.fi

Yliopistopaino
Helsinki 2008

List of Publications

[1] Y.-C. Lin, J. Jusélius, D. Sundholm, and J. Gauss, "Magnetically Induced Current Densities in Al_4^{2-} and Al_4^{2-} Species Studied at the Coupled-Cluster Level," J. Chem. Phys., vol. 122, p. 214308, 2005.

[2] Y.-C. Lin, D. Sundholm, J. Jusélius, L.-F. Cui, X. Li, H. J. Zhai, and L.-S. Wang, "Experimental and Computational Studies of Alkali-Metal Coinage-Metal Clusters," J. Phys. Chem. A, vol. 110, p. 4244, 2006.

[3] Y.-C. Lin and D. Sundholm, "On the Aromaticity of the Planar Hydrogen-Bonded $(HF)_3$ Trimer," J. Chem. Theory Comput., vol. 2, p. 761, 2006.

[4] L.-F., Cui, Y.-C. Lin, D. Sundholm, and L.-S. Wang, "A Photoelectron Spectroscopic and Computational Study of Sodium Auride Clusters, $Na_nAu_n^-$ (n = $1-3$)," J. Phys. Chem. A, vol. 111, p. 7555, 2007

Acknowledgements

The studies in this thesis were performed under the supervision of Dage Sundholm. I feel an immense gratitude to him who has all the qualities of a great supervisor. More than being an excellent scientist, he also has guided me with kindness and passion. I would like to thank Pekka Pyykkö for being a wise group leader of the Laboratory for Instruction in Swedish. He amazes me with his tremendous knowledge of chemistry.

The referees of my thesis, Nino Runeberg and Perttu Lantto, have given me useful and constructive comments on the manuscript for which I am grateful. I thank Antonio Rizzo and Chao-Ping Hsu for sharing their experience in science with me during my stays in Pisa and in Taipei. Also, it has been my pleasure to work with my co-authors, and I thank them for the collaboration. I am obliged to the NANOQUANT - EU FP6 RTN network and Graduate School of Computational Chemistry and Molecular Spectroscopy for the financial support.

I am glad work in the group with a cordial atmosphere; for this, I would like to show my appreciation to all my colleagues: Henrik Konschin, Juha Varaa, Michal Straka, Jonas Jusélius, Mikael Johansson, Michael Patzschke, Olli Lehtonen, Sebastian Riedel, Michiko Atsumi, Stefan Taubert, Tommy Vänskä, Patryk Zaleski Ejgierd, Cong Wang, Sergio Losilla, Bertel Westermark, Anneka Tuomola, Nina Siegfrids, Susanne Lundberg, Bjarne Lindström and Raija Eskelinen. I specially thank Jonas for being a nice senior, Stefan for being a good friend and Susanne for being a warm person. In addition, many thanks to those who spent time on revising my manuscripts.

My life in Helsinki would not be this wonderful without my parents, three younger sisters, grandparents and friends in Taiwan and elsewhere in the world. I owe a deep gratitude to them for sending me lovely letters and parcels, for visiting me even from the other side of the Earth, for being on-line whenever I needed, and most importantly for caring about me. I cherish everything they have given me. At last, I would like to convey my love to Ari who always stands by me.

Contents

Chapter 1

Introduction

THE bimetallic clusters have attracted considerable attention due to the potential technological applications of mixed-metal systems and their aberrant catalytic properties as compared to monometallic catalysts [5]. For example, the high catalytic activity of nanosized gold clusters and gold islands on carrier surfaces suggests that cold-containing bimetallic clusters can be ecient catalysts [6]. Solid alkali-auride compounds such as CsAu and RbAu have been extensively studied to ascertain the nature of the alkali-gold bonds [7, 8, 9, 10, 11, 12, 13, 14] . Their studies showed that the electric properties change intensely along the alkali metal series from Na to Rb. CsAu and RbAu are ionic semiconductors, whereas the lighter alkali-auride solids are metals [8]. The stability of the diatomic alkali-auride compounds in the gas phase have been investigated experimentally using mass-spectrometry analysis of vapor compositions and by two photon ionization measurements [15, 16, 17, 18, 19, 20, 21] . One of the studies included in this thesis is to investigate sodium auride by performing quantum chemical calculations. Our calculations together with experimental photoelectron spectroscopic (PES) studies are able to characterize the molecular structures of these newly generated clusters [2, 22].

As described in most organic chemistry textbooks nowadays, a group of compounds are classified as aromatic compounds because of their remarkable stabilities, particular geometrical and energetic properties and so on. The notion of aromaticity is essentially qualitative. The Hückel's rule was the first quantitative approach to describe aromaticity. Later, it was followed by the definition of resonance energy (RE) by Pauling and Sherman [23, 24]. More recently, attempts have been made to connect aromaticity with energetic and magnetic properties, such as electric polarisabilities, hyperpolarisabilities, magnetic susceptibilities, nuclear magnetic shieldings, and nuclear spin-spin coupling constants. Based on these, there are various aromaticity indices proposed to examine the aromaticity magnitude: aromatic stabilization energies (ABE) [25]; nucleus-independent chemical shifts (NICS) [26]; aromaticity methods derived from the ring-current model (RCM) [23, 24, 25, 27, 28, 29, 30, 31, 32, 33, 34]. Computational chemists introduced more aspects on the subject; the discussions of the aromatic nature of molecular rings are no longer limited to organic compounds obeying the Hückel's rule. By applying several aromaticity criteria, the magnetic properties of Al_4^{2-}, Al_4^{4-}, Cu_4^{2-} and $(HF)_3$ have been calculated in order to understand the nature of aromaticity of these clusters [1, 2, 3].

Chapter 2

Theory: Molecular Energies

ONE of the most important theoretical bases in computational chemistry is quantum mechanics. By 1926, Heisenberg and Schrödinger had built the non-relativistic mathematical models for describing the motion of nuclei and electrons in molecules [35, 36]. The difference between these two models is only in how time is specified. In the Heisenberg picture, time dependence is possessed in the operators whereas time is carried in state vectors in the Schrödinger picture. Time-dependent and time-independent Schrödinger equations are respectively formulated as $i\frac{\partial\Psi}{\partial t} = \hat{H}\Psi$ and $\hat{H}\Psi = E\Psi$ where $\hat{H}$ is the Hamiltonian, Ψ is the wave function, and E is the total energy of the molecular system. Shortly afterwards, a relativistic generalized equation was proposed by Dirac [37]. The concept of theoretical investigation on molecular systems has been important ever since. However, it is impossibe to analytically solve the exact wavefunction for any system other than the one-electron hydrogen atom and the H_2^+ molecule. It was also stated by Dirac in 1929 [38] that "The underlying physical laws necessary for the mathematical theory of a large part of physics and the whole of chemistry are thus completely known, and the difficulty is only that the exact application of these laws leads to equations much too complicated to be soluble." Over the past decades, a considerable number of attempts have been made not only to solve the wavefunctions approximately but also to construct expressions for calculations of electron densities instead. The latter approach is the so-called Density Functional Theory (DFT) method [39].

2.1 Approximate Wavefunctions

We shall introduce the often used non-relativistic Hamiltonian and leave out the discusstions on other Hamiltonians which treat many-electron systems relativistically. Within the framework of Born-Oppenheimer approximation [40], the nonrelativistic and spin-free molecular electronic Hamiltonian in the orbital basis can be expressed in the language of second quantization as

$$\hat{H} = \sum_{pq} h_{pq}\hat{E}_{pq} + \frac{1}{2}\sum_{pqrs} g_{pqrs}\hat{e}_{pqrs} + h_{\text{nuc}} \tag{2.1}$$

In Eq. 2.1, one- and two-electron operators are represented by the products of creation $a^\dagger$ and annihilation a operators obeying the fermionic anticommutation rules: $\hat{E}_{pq} = a^\dagger_{p\alpha}a_{q\alpha} + a^\dagger_{p\beta}a_{q\beta}$ and $\hat{e}_{pqrs} = \hat{E}_{pq}\hat{E}_{rs} - \delta_{qr}\hat{E}_{ps} = \sum_{\sigma\tau} a^\dagger_{p\sigma}a^\dagger_{r\tau}a_{s\tau}a_{q\sigma}$. One- and two-electron integrals h_{pq}

and g_{pqrs} are defined as

$$h_{pq} = \int \phi_p^*(\boldsymbol{x})(-\frac{1}{2}\nabla^2 - \sum_I \frac{Z_I}{|\mathbf{R}_I - \mathbf{r}|})\phi_q(\boldsymbol{x})\mathrm{d}\boldsymbol{x} \tag{2.2}$$

$$g_{pqrs} = \int\int \frac{\phi_p^*(\boldsymbol{x}_1)\phi_q(\boldsymbol{x}_1)\phi_r^*(\boldsymbol{x}_2)\phi_s(\boldsymbol{x}_2)}{|\mathbf{r}_1 - \mathbf{r}_2|}\mathrm{d}\boldsymbol{x}_1\mathrm{d}\boldsymbol{x}_2 \tag{2.3}$$

where the integrations are over spatial degress of freedom. The last term h_{nuc} denotes the nuclear-repulsion energy. This Hamiltonian omits interactions which are assumed to be small such as relativistic effects, spin-orbital interaction and Lamb shift. Relativistic effects in our studies were taken into account by empolying effective core potentials (ECPs) meaning that the core electrons in a calculation are replaced with an effective potential. In addition, the need for the core basis functions can be eliminated.

The molecular electronic wavefunctions $|\mathrm{CSF}\rangle$ are popularly constructed from N-electron Slater determinants, and each determinant represents an antisymmetric product of one-electron orbitals to fulfill the antisymmetry condition of fermions . The total energy of the molecular system can be then obtained as

$$E = \sum_{pq} D_{pq}h_{pq} + \frac{1}{2}\sum_{pqrs} d_{pqrs}g_{pqrs} + h_{\mathrm{nuc}} \tag{2.4}$$

where D_{pq} and d_{pqrs} are one- and two-electron density matrices which are defined as $D_{pq} = \langle\mathrm{CSF}|\,\hat{E}_{pq}\,|\mathrm{CSF}\rangle$ and $d_{pqrs} = \langle\mathrm{CSF}|\,\hat{e}_{pqrs}\,|\mathrm{CSF}\rangle$. One can, of course, approach the exact solution to the Schrödinger equation by systematically improving the one-partical basis and N-electron description, but in most cases it is not possible due to the expensive computational costs. In this section, several standard methods of constructing approximate electronic wavefunctions are briefly delineated in order to provide the background for the calculations included in the thesis. The details of the theories and the relevant equations presented in this section can be found in several publications [41, 42, 43, 44, 45, 46, 47, 48, 49].

THE HARTREE-FOCK SELF CONSISTENT-FIELD METHOD

For many-electron systems, the idea of the self consistent field (SCF) method was originally introduced by Hartree in 1928. He first constructed the many-electron wavefunction as a product of hydrogenlike orbitals and then continued to calculate improved orbitals from an effective one-electron equation until there is no further change in the orbitals. Later in 1930, Fock and Slater pointed out that one must use an antisymmetric linear combination of products of spin-orbitals instead [50]. Since then, the SCF approach has been implemented in most quauntum chemistry programs.

In most applications, the Molecular Orbitals (MOs) ϕ_p are expanded in a set of atomic orbitals (AOs) or basis functions χ_μ. A set of contracted Gaussian functions: $\phi_p = \sum_\mu \chi_\mu C_{\mu p}$ is usually used to span the MOs. The expansion coefficients can be used as variational parameters when imposing the orthonormalization conditions on the orbitals. The so-called Roothaan-Hall equations [51, 52] on the HF method can be then represented as a generalized eigenvalue expression

$$\mathbf{FC} = \mathbf{SC}\varepsilon \tag{2.5}$$

where $\mathbf{F}$ is the Fock matrix, $\mathbf{C}$ the coefficient matrix, $\mathbf{S}$ the overlap matrix of AO basis functions, and ε a diagonal matrix containing the orbital energies. For a closed-shell system, the

Fock matrix elements can be calculated as

$$f_{\mu\nu}^{\mathrm{AO}} = h_{\mu\nu} + \sum_i (2g_{\mu\nu ii} - g_{\mu iiv}) = h_{\mu\nu} + \sum_{\rho\sigma} D_{\rho\sigma}^{\mathrm{AO}} (g_{\mu\nu\rho\sigma} - \frac{1}{2} g_{\mu\sigma\rho\nu}) \tag{2.6}$$

where the AO density matrix $D_{\rho\sigma}^{\mathrm{AO}}$ is defined as $2\sum_i C_{\rho i} C_{\sigma i}$. An iterative process can be performed by recalculating the Fock matrix from a given set of MOs. The eigenvalue problem yields a new set of orbitals and the corresponding density matrix. This cycle is then repeated until the solution is practically unchanged in two subsequent iteration cycles. The use of the expression in the AO basis avoids the expensive transformations of the two-electron integrals to the MO basis [41]. An improved Fock operator can be generated by averaging over the MO coefficients of the current and the previous iteration steps in order to stabilize the iterative procedure. A popular and successful approach to stabilize and speed up the solution of the SCF equation is known as the direct inversion in the iterative subspace (DIIS) method [53, 54].

The optimization of the HF wavefunction by the SCF procedure sometimes fails to converge even with the DIIS method. In such cases, one should apply a second-order optimization such as the Newton method which is based on a local quadratic model of the energy surface. The Newton step is obtained by solving a set of linear equations involving the Hessian matrix. With the Roothaan-Hall method, the cost of the diagonalization of the Fock matrix scales cubically with the size of the system ($\sim N^3$) making it less useful for very large systems. The density-based optimization method thereby becomes a better choice than the Roothaan-Hall method because the computational cost can be made to scale only linearly with the size of the system [55, 56, 57, 58, 59, 60].

The energy difference between the HF and the exact solutions is defined as the correlation energy in the non-relativistic scheme [61]. The HF wavefunction is often considered as a reference function for electron correlation methods in order to acquire accurate correlation energy. However, this is not an option if the electronic wave functions are dominated by more than one electronic configuration, *i.e.* a single determinant is no longer enough to qualitatively describe the wavefunction. Cases in point of this problem are the investigations into the electronic ground state of the ozone molecule and the dissociation of the nitrogen molecule. For such studies, the multiconfigurational self-consistent field (MCSCF) method should be applied to replace the HF wavefunction as a starting point. The details of the MCSCF method are not dicscussed here.

CONFIGURATION-INTERACTION THEORY

The configuration-interaction (CI) wave function consists of a linear combination of Slater determinants:

$$|\mathrm{CI}\rangle = \sum_i c_i |i\rangle \tag{2.7}$$

with the expansion coefficients c_i. The CI coefficients are variationally determined leading to an eigenvalue problem for the coefficients and the energy.

$$\mathbf{H}\mathbf{C}_{\mathrm{CI}} = \mathbf{E}\mathbf{C}_{\mathrm{CI}} \tag{2.8}$$

In Eq. 2.8, $\mathbf{H}$ is the Hamiltonian matrix with the matrix elements $H_{ij} = \langle i| \hat{H} |j\rangle$ and $\mathbf{C}_{\mathrm{CI}}$ is a vector containing the expansion coefficients c_i. In the full CI (FCI) model, the complete set of determinants generated by distributing all electrons among all orbitals is considered.

The correlation energy is defined as the difference between the FCI and the Hartree-Fock energies and the FCI model has been used to provide benchmarks for other approximate wavefunction models for small systems. With increasing number of electrons and orbitals, the FCI wave functions become intractable due to the enormous number of determinants. A straightforward solution to this shortcoming is to obtain approximate CI wavefunctions by truncating the FCI expansion. There are several different ways of trunctations, and the techniques can be then chosen according to the treatments of static correlation, dynamic correlation or both. For example, a large part of the dynamic correlation energy can be recovered by including all configurations generated by excitations out of the reference space such as all single and double excitations (CISD). However, one should be aware that the size-extensivity of the FCI wave functions is destroyed by the truncation.

COUPLED-CLUSTER THEORY

The coupled-cluster (CC) wave function [41, 42, 62] is an alternative of the wave function expressions which can be extended to the exact wave function. While the CI method is based on a linear parametrization, the CC wavefunction can be written as an exponential ansatz for the wavefunction:

$$|\mathrm{CC}\rangle = e^{\hat{T}} |\mathrm{HF}\rangle \tag{2.9}$$

where the cluster operator for a n-electron system is defined as a linear combination of excitation operators multiplied by the corresponding connected cluster amplitudes: $\hat{T} = \hat{T}_1 + \hat{T}_2 + \cdots + \hat{T}_i$ with $\hat{T}_i = \sum_{\nu_i} t_{\nu_i} \tau_{\nu_i}$. The label ν_i refers to an ordering with respect to excitation levels i and numbering ν within excitation classes. The full coupled-cluster (FCC) wave function is implicitly equivalent to the FCI wave function: $e^{\hat{T}} |\mathrm{HF}\rangle = \sum_{i=o}^{N} \hat{C}_i |\mathrm{HF}\rangle$.

$$e^{\hat{T}} = \underbrace{1}_{\hat{C}_0} + \underbrace{\hat{T}_1}_{\hat{C}_1} + \underbrace{\hat{T}_2 + 1/2\hat{T}_1^{\,2}}_{\hat{C}_2} + \underbrace{\hat{T}_3 + \hat{T}_1\hat{T}_2 + 1/6\hat{T}_1^{\,3}}_{\hat{C}_3} + \cdots \tag{2.10}$$

The main advantage is that the exponential ansatz automatically generates all disconnected clusters (the product of the lower-order excitation amplitudes) even at the truncated level. Only the connected terms, such as $\hat{T}_1$, $\hat{T}_2$, $\hat{T}_3 \cdots$, are missing according the choice of the truncation. Some of the higher-order excitations are implicitly considered in the coupled-cluster calculations.

The full coupled-cluster wavefunction satisfies the Schrödinger equation:

$$\hat{H}e^{\hat{T}} |\mathrm{HF}\rangle = Ee^{\hat{T}} |\mathrm{HF}\rangle \tag{2.11}$$

The variational minimization of the coupled-cluster wave function is more complicated than the one for the CI energy expression. Projections of the Schrödinger equation onto the HF wavefunction and onto the determinant $|\mu\rangle$ give an non-variational expression for the coupled-cluster energy and the coupled-cluster equations for the amplitudes:

$$\langle \mathrm{HF}| \hat{H}e^{\hat{T}} |\mathrm{HF}\rangle = E \tag{2.12}$$

$$\langle \mu| \hat{H}e^{\hat{T}} |\mathrm{HF}\rangle = E \langle \mu| e^{\hat{T}} |\mathrm{HF}\rangle \tag{2.13}$$

The values for the amplitudes can be obtained by iteratively solving Eq. 2.13, whose energy is taken from Eq. 2.12. The Schrödinger equation (Eq. 2.11) can be reformulated by

multiplying it from the left with the operater $e^{-\hat{T}}$:

$$e^{-\hat{T}}\hat{H}e^{\hat{T}}\left|\mathrm{HF}\right\rangle = E\left|\mathrm{HF}\right\rangle \tag{2.14}$$

In Eq. 2.14, $\hat{H}^{\mathrm{T}} = e^{-\hat{T}}\hat{H}e^{\hat{T}}$ is an effective , non-Hermitian similarity-transformed Hamiltonian. A new set of equations for the coupled-cluster amplitudes and energy can then be written as

$$\left\langle \mathrm{HF}\right| \hat{H}^{\mathrm{T}}\left|\mathrm{HF}\right\rangle = E \tag{2.15}$$

$$\left\langle \mu\right| \hat{H}^{\mathrm{T}}\left|\mathrm{HF}\right\rangle = 0 \tag{2.16}$$

Size-extensivity is achieved no matter how thet excitation operators in $\hat{T}$ are truncated in the so-called similarity-transformed, linked formulation of the CC framework. A great advantage of the coupled-cluster approach is that it gives a systematic hierarchy of well-defined black-box methods with increasing computational accuracy. In the sequence of CCS, CC2, CCSD, CCSD(T), CC3, CCSDT models, higher order excitation amplititudes are considered yielding better accuracy and also higher computational costs [63, 64]. The CCS model is a standard coupled-cluster model with only $\hat{T}_1$ included; D and T denote the addition of $\hat{T}_2$ and $\hat{T}_3$, respectively. The approximate coupled-cluster singles and doubles (CC2) model is obtained by a different treatment of $\hat{T}_1$ and $\hat{T}_2$, and it is distinguished from the CCSD model by the fact that the CC2 doubles equations are approximated to be correct through first order in the fluctuation potential [65]. The CC2 amplitude equation can be written as

$$\begin{array}{l} \left\langle \mu_1\right| \hat{H} + \left[\hat{H}, \hat{T}_2\right]\left|\mathrm{HF}\right\rangle = 0 \\ \left\langle \mu_2\right| \left[\hat{F}, \hat{T}_2\right] + \hat{H}\left|\mathrm{HF}\right\rangle = 0 \end{array} \tag{2.17}$$

with a Fock operator $\hat{F}$ defined as the difference between Hamiltonian $\hat{H}$ and a fluctuation potential. The CC3 model is analogously approximated from the CCSDT model by retaining those terms which are of second order in the fluctuation potential in the triplet equations. The same manner as for the CCSDT model is then proceeded *i.e.* the CCSDT (or CC3) equations are solved iteratively until convergence. A popular non-interative approximation to CCSDT is the CCSD(T) model — it is constructed to achieve the same improvement as CC3 in energy by adding the necessary corrections to the CCSD energy directly from perturbation theory by examining the lowest-order terms that contain connected triplets [66, 67].

Rather accurate molecular electronic coupled-cluster energies can be calculated using such a nonvariational projection approach. However, the calculations of molecular properties are more difficult at the coupled-cluster level as the conditions for the Hellmann-Feynman theorem are not readily fulfilled. The solution to this problem is to construct a variational Lagrangian [68, 69] for the coupled-cluster theory. In the presence of a perturbation $\alpha\hat{V}$, a generalization of the Hellmann-Feynman theorem to coupled-cluster wave functions can be then established as

$$\begin{array}{rcl} \left.\frac{\mathrm{d}E}{\mathrm{d}\alpha}\right|_{\alpha=0} & = & \frac{1}{2}\left\{\left[\left\langle \mathrm{HF}\right| + \sum_{\nu}\bar{t}_{\nu}^{(0)}\left\langle \nu\right| e^{-\hat{T}^{(0)}}\right]\hat{V}\left|\mathrm{CC}\right\rangle + \left[\left\langle \mathrm{HF}\right| + \sum_{\nu}\bar{t}_{\nu}^{(0)}\left\langle \nu\right| e^{-\hat{T}^{(0)}}\right]\hat{V}\left|\mathrm{CC}\right\rangle^{*}\right\} \\ & = & \frac{1}{2}\left[\left\langle \Lambda\right|\hat{V}\left|\mathrm{CC}\right\rangle + \left\langle \Lambda\right|\hat{V}\left|\mathrm{CC}\right\rangle^{*}\right] \end{array} \tag{2.18}$$

where $\hat{T}^{(0)}$ is the cluster operator and $\bar{t}_{\nu}^{(0)}$the Lagrange multipliers in the absence of the perturbation. In principle, a calculation for each excited state of interest can be carried out separately by applying an appropriate zeroth-order reference determinant, but several problems come along with this direct strategy. It starts with a difficult and often impossible search for a suitable zeroth-order reference determinant for a excited state; the individual calculation

of each state is as demanding as one for the ground state; moreover, the excited states are generated in such a way that they are not orthogonal meaning that they are not easy to be identified [41]. One possibility of calculating the excited states within the coupled-cluster theory is to see the excited states as a linear expansion in the space spanned by all states of the form containing the coupled-cluster ground state $|\mathrm{CC}\rangle$. They are called the equation-of-motion coupled-cluster (EOM-CC) excited states [70]:

$$|\mathbf{c}) = \sum_{\mu} c_{\mu} \hat{\tau}_{\mu} |\mathrm{CC}\rangle = e^{\hat{T}} \sum_{\mu} c_{\mu} \hat{\tau}_{\mu} |\mathrm{HF}\rangle = \sum_{\mu} c_{\mu} |\mu) \tag{2.19}$$

where the summation is over the identity operator $\hat{\tau}_0$ and over the excitation operator present in the cluster operator $\hat{T}$. The EOM-CC energy can be expressed as a pseudo-expectation value or an expectation value associated with the similarity-transformed Hamiltonian.

$$E(\mathbf{c}, \bar{\mathbf{c}}) = \frac{(\bar{\mathbf{c}}| \hat{H} |\mathbf{c})}{(\bar{\mathbf{c}} \mid \mathbf{c})} = \frac{\langle \bar{\mathbf{c}}| \hat{H}^{\mathrm{T}} |\mathbf{c}\rangle}{\langle \bar{\mathbf{c}} \mid \mathbf{c}\rangle} \tag{2.20}$$

where $(\bar{\mathbf{c}}|$ is defined as $\sum_{\mu} \bar{c}_{\mu} \langle HF| \hat{\tau}_{\mu}^{\dagger} e^{-\hat{T}} = \sum_{\mu} \bar{c}_{\mu} (\mu|$. The overbars are used for bra coefficients. They differ numerically from the coefficients of the ket vectors. The similarity-transformed Hamiltonian matrix elements referring to the excited projection manifold can be derived as

$$H_{\mu v} = (\mu| \hat{H} |v) = \langle \mathrm{HF}| \hat{\tau}_{\mu}^{\dagger} \hat{H}^{\mathrm{T}} \hat{\tau}_{v} |\mathrm{HF}\rangle = (\mu| \left[\hat{H}, \hat{\tau}_{v}\right] |\mathrm{HF}) + \delta_{\mu v} E_0 \tag{2.21}$$

The term $\delta_{\mu v} E_0$ in Eq. 2.21 is obtained with the use of the resolution-of-the-identity (RI) approximation [71]. Proved as an efficient technique of reducing calculation time, the RI approximation has been widely invoked in some other coupled-cluster models as well as in the second-order Møller-Plesset perturbation theory (MP2) and the DFT methods. Before discussing the excited-state solutions to the EOM-CC eigenvalue equations, we can first take a look at the EOM-CC Hamiltonian in the partition form for an optimized coupled-cluster state [41].

$$\mathbf{H} = \begin{pmatrix} 0 & \boldsymbol{\eta}^{\mathrm{T}} \\ \mathbf{0} & \mathbf{A} \end{pmatrix} + E_0 \mathbf{1} \tag{2.22}$$

where the elements of the column vector $\boldsymbol{\eta}$ and the elements of the coupled-cluster Jacobian matrix $\mathbf{A}$ are given in the following:

$$\eta_{\mu} = (\mathrm{HF}| \hat{H} |\mu) \tag{2.23}$$

$$A_{\mu v} = (\mu| \left[\hat{H}, \hat{\tau}_{v}\right] |\mathrm{HF}) \tag{2.24}$$

The EOM-CC eigenvalue problem can first be obtained by differentiating Eq. 2.20 with respect to the $(\bar{\mathbf{c}}|$ and $|\mathbf{c})$ coefficients; then, the excitation energies are obtained by solving the corresponding level-shifted equations:

$$\begin{array}{c} \mathbf{H}\mathbf{c} = E\mathbf{c} \\ \bar{\mathbf{c}}^{T}\mathbf{H} = \bar{\mathbf{c}}^{T}E \end{array} \implies \begin{array}{c} \boldsymbol{\Delta}\mathbf{H}\mathbf{c} = \Delta E\mathbf{c} \\ \bar{\mathbf{c}}^{T}\boldsymbol{\Delta}\mathbf{H} = \bar{\mathbf{c}}^{T}\Delta E \end{array} \tag{2.25}$$

where the Hamiltonian $\boldsymbol{\Delta}\mathbf{H}$ is obtained as $\mathbf{H} - E_0\mathbf{1}$ and the energy difference ΔE is given by $E - E_0$ meaning that the nonzero eigenvalues correspond to the excitation energies from the ground state. A pair of eigenvectors can be chosen in form of

$$\mathbf{c} = \begin{pmatrix} s \\ \mathbf{t} \end{pmatrix}, \bar{\mathbf{c}} = \begin{pmatrix} \bar{s} \\ \bar{\mathbf{t}} \end{pmatrix} \tag{2.26}$$

where s and $\bar{s}$ are the coefficients associated with the reference state $\mu = 0$ and, on the other hand, $\mathbf{t}$ and $\bar{\mathbf{t}}$ for the excited configurations $\mu > 0$. The excited-state solution for the k-th state to the EOM-CC eigenvalue equations can then be solved. The excitation energies are finally obtained as

$$\mathbf{A}\mathbf{t}_k = \Delta E_k \mathbf{t}_k,\ \bar{\mathbf{t}}_\mathbf{k}^\mathrm{T}\mathbf{A} = \bar{\mathbf{t}}_k^\mathrm{T}\Delta E_k \tag{2.27}$$

and the coefficients for the reference-state are given by

$$s_k = \Delta E_k^{-1}\boldsymbol{\eta}^\mathrm{T}\mathbf{t}_k,\ \bar{s}_k = 0 \tag{2.28}$$

The key factor is that the first column vector of the EOM-CC Hamiltonian $\mathbf{\Delta H}$ vanishes so that excitation energies can be calculated as eigenvalues of the Jacobian $\mathbf{A}$. For the standard coupled-cluster model (CCSD and CCSDT) whose first column contains Eq. 2.16, this condition is satisfied. The EOM-CC theory can therefore be applied at the standard CC models. Other than EOM-CC application, the excitation energies and the transition moments can also be defined by deriving CC response funcitons in a form which is compatible with the structure of the exact response function [72]. In the presence of a time-dependent one electron perturbation $\hat{V}^t$, the system can be defined as $\hat{H} = \hat{H}_0 + \hat{V}^t$ where $\hat{H}_0$ contains the Fock operator and the fluctuation potential. With the quasienergy approach, the linear response function can be written as

$$\begin{aligned}
\left\langle\left\langle \hat{V}^A; \hat{V}^B \right\rangle\right\rangle_\omega &= \left.\frac{\partial^2\{L\}_T}{\partial\epsilon_A(-\omega)\partial\epsilon_B(\omega)}\right|_0 \\
&= \langle\Lambda|\left[\hat{V}^A, \hat{T}^B(\omega)\right]|\mathrm{CC}\rangle + \langle\Lambda|\left[\hat{V}^B, \hat{T}^A(\omega)\right]|\mathrm{CC}\rangle \\
&+ \langle\Lambda|\left[\left[H_0, \hat{T}^A(\omega)\right], \hat{T}^B(\omega)\right]|\mathrm{CC}\rangle
\end{aligned} \tag{2.29}$$

where $\{L\}_T$ denotes the time-averaged Largrangian. The equations for the cluster amplitudes t are obtained from the variational requirement:

$$(\omega\mathbf{1} - \mathbf{A})\,\mathbf{t}^A = -\boldsymbol{\xi}^A \tag{2.30}$$

and the zeroth-order multipliers are determined from

$$\bar{\mathbf{t}}^{(0)}\mathbf{A} = \boldsymbol{\zeta}^{(0)} \tag{2.31}$$

where $\mathbf{A}$ is the CC Jacobian whereas $\boldsymbol{\xi}^A$ and $\boldsymbol{\zeta}^{(0)}$ are the corresponding vectors. Excitation energies and transition moments can be calculated as poles and residues of the linear response function. The poles of the response function occur at the poles of the amplitude responses [72, 73]. The CC excitation energies can thereby be determoned as

$$\mathbf{A}\mathbf{S}_k = \omega_k\mathbf{S}_k \tag{2.32}$$

The advantage of this approach is that it can be applied to approximate coupled-cluster models. Take the CC2 model as an example, the vectors $\boldsymbol{\xi}^A$ and $\boldsymbol{\zeta}^{(0)}$ can be defined as

$$\begin{aligned}
\boldsymbol{\xi}^A &= \begin{pmatrix} \langle\mu_1|\,\hat{V}^A + \left[\hat{V}^A, \hat{T}_2^{(0)}\right]|\mathrm{HF}\rangle \\ \langle\mu_2|\left[\hat{V}^A, \hat{T}_2^{(0)}\right]|\mathrm{HF}\rangle \end{pmatrix} \\
\boldsymbol{\zeta}_{\nu_i}^{(0)} &= \langle\mathrm{HF}|\left[\hat{H}_0, \tau_{\nu_i}\right]|\mathrm{HF}\rangle
\end{aligned} \tag{2.33}$$

PERTURBATION THEORY

The coupled-cluster method can be applied to yield calculation results of chemical accuracy. However, the computational costs may not be affordable for extended systems, and it would be profitable to canvass some other approaches such as perturbation theory. The basic idea of the perturbation theory is to partition the Hamiltonian into the zeroth-order Halmiltonian $\hat{H}_0$ and the pertubation, and then to expand the eigenfunction of the exact Hamiltonian $\hat{H}$ with the eigensolutions to $\hat{H}_0$.

In order to calculate the correlation energy, the zero-order Hamiltonian is commonly chosen as the Fock operator, the zero-order states are then presented by the Hartree-Fock determinant and the determinants excited with respect to this state. This is known as Møller-Plesset perturbation theory (MPPT) [74]. The perturbation (also referred as the fluctuation potential $\hat{\Phi}$) represents the difference between the averaged and instantaneous interactions [41]. We can now make a perusal of the systematic scheme. The first-order wave function correction $|\text{MP1}\rangle$ can be regarded as $\hat{T}_2^{(1)}|\text{HF}\rangle$ where the perturbation operator $\hat{T}_2^{(1)}$ is a linear combination of excitation operators multiplied by a first-order amplitude; the second-order correction $|\text{MP2}\rangle$ involves single, double, triple and quadruple excitations from the Hartree-Fock state: $|\text{MP2}\rangle = \left(\hat{T}_1^{(2)} + \hat{T}_2^{(2)} + \hat{T}_3^{(2)} + \hat{T}_4^{(2)}\right)|\text{HF}\rangle$. The second-order quaduple excitation $\hat{T}_4^{(4)}$ can be represented as $\frac{1}{2}\hat{T}_2^{(1)^2}$ being the only disconnected term in the MP2 wavefunction. The corresponding energy corrections can be written in a form of

$$E_{\text{MP}}^{(1)} = \langle \text{HF}|\,\hat{\Phi}\,|\text{HF}\rangle\,,\; E_{\text{MP}}^{(2)} = \langle \text{HF}|\left[\hat{H}, \hat{T}_2^{(1)}\right]|\text{HF}\rangle \tag{2.34}$$

In commutator expressions, the energy corrections are termwise separable and the wave funcitons are size-extensive. Explicit expressions for the second-order energy correction $E_{\text{MP}}^{(2)}$ in terms of integrals and orbital energies is given by

$$E_{\text{MP}}^{(2)} = -\sum_{\substack{a>b\\ i>j}} \frac{\left|g_{aibj} - g_{ajbi}\right|^2}{\varepsilon_a + \varepsilon_b - \varepsilon_i - \varepsilon_j} \tag{2.35}$$

where g are the two-electron integrals and ε are the orbital energies. The MP2 energy denotes the total energy obtained with the inclusion of all corrections up to second order:

$$E_{\text{MP2}} = E_{\text{MP}}^{(0)} + E_{\text{MP}}^{(1)} + E_{\text{MP}}^{(2)} + h_{nuc} = E_{\text{HF}} + E_{\text{MP}}^{(2)} \tag{2.36}$$

It can be noticed that both CC and MPPT approaches use HF wave function as reference indicating that they in general cannot be applied to systems with degenerate or nearly degenerate electronic configurations. One can then introduce multiconfigurational SCF wavefunctions such as the complete-active-space (CAS) SCF wave functions. The static correlation is taken care of by employing multiconfiguration wave functions. Within the CAS framework, the core orbitals of any system are usually treated as inactive and the valence orbitals as active [75]. The CAS perturbation theory (CASPT) is currently the most applicable method of taking dynamic effects into account for such systems.

2.2 Density Functional Theory

Being the founders of modern density functional theory, Hohenberg and Kohn proved in 1964 that all ground-state properties are uniquely determined by the ground-state electron

probability density $\rho_0(x, y, z)$ which is a function of only three variables for molecules with a nondegenerate ground state [76]. Kohn and Sham later took a long step forward presenting a method for finding ρ_0 without first solving the wave function and for finding E_0 from ρ_0 [77]. The formulation of the Kohn-Sham equation is similar to the SCF equation. The main difference between Hartree-Fock (HF) and Kohn-Sham (KS) equations is that the exchange term in HF is replaced by the exchange-correlation potential $v_{xc}(\mathbf{r})$ representing the exchange-correlation energy $E_{xc}[\rho]$[78].

The subject of density functional theory has been well elaborated for decades [39]. If the true functional could be found, the energy obtained by the KS method would be the same as the eigenvalue of the Schrödinger equation. However, the exact $E_{xc}[\rho]$ is unfortunately unknown; finding (designing) suitable approximations for $E_{xc}[\rho]$ becomes an important task in modern DFT theory. One should keep in mind that there is no methodical nor systematical scheme of how to construct more accurate $E_{xc}[\rho]$ whereas the accuracy is correspondingly improved with better description of the molecular wave functions. The application of DFT must be thus carried out with attentions on the choice of functionals. DFT has the advantage that correlation effects are included in a calculation that takes much less time compared with *ab initio* electron correlation methods, and it can therefore be applied on large systems.

Chapter 3

Theory: Molecular Properties

BESIDES the energy of the molecular systems, various molecular properties such as molecular structures, excitation energies, vibrational frequencies, nuclear magnetic shieldings and magnetically induced currents have been investigated in this thesis. A general expression of molecular properties calculated as energy derivatives is first introduced in this chapter, . Then it is applied on several aspects of magnetic properties, and finally to the magnetic criteria for aromaticity.

3.1 Molecular Properties Calculated as Energy Derivatives

When the molecular system is affected by an external perturbation and the perturbation is small, the change in the total energy can be expressed as a power series in the perturbation

$$E(\lambda) = \lambda E^{(1)} + \lambda^2 E^{(2)} + ..., \tag{3.1}$$

where λ is a parameter that characterizes the perturbation, and the coefficients $E^{(n)}$ are the $n : th$ derivative of the energy representing the response of the system to the external perturbation [48, 79, 80]. The $E^{(n)}$ are usually known as the $n : th$ order molecular observables.

$$E^{(n)} = \frac{1}{n!}\frac{d^n E(\lambda)}{d\lambda^n} \tag{3.2}$$

A first-order property, which is linearly dependent on λ, can be deduced from the first derivative of the energy

$$\left.\frac{dE(\lambda)}{d\lambda}\right|_{c=c'} = \left.\frac{\partial E(\lambda;c)}{\partial\lambda}\right|_{c=c'} + \left.\frac{\partial E(\lambda;c)}{\partial c}\frac{\partial c}{\partial\lambda}\right|_{c=c'} \tag{3.3}$$

where c is a set of wave-function or electronic parameters that determines the electronic state. Both terms on the right-hand side of Eq. 3.3 represent the dependence of the electronic energy as a function of λ: the former arises from the dependence of the energy on the perturbation when assuming that the wave function is not affected by the external field, whereas the later arises since the electronic structure *via* the molecular orbitals (MO) and configuration parameters change due to the perturbation.

Here we assume that the electronic energy for the unperturbed situation is fully variational with respect to the electronic parameters c. The electronic energy can then be calculated as

$$E(\lambda) = E(\lambda; c') \tag{3.4}$$

where the parameters c' represent the optimal value of c. The optimized energy function $E(\lambda; c')$ satisfies the variation conditions for all state parameters

$$\left.\frac{\partial E(\lambda; c)}{\partial c}\right|_{c=c'} = 0 \tag{3.5}$$

By combining Eq. 3.3 and Eq. 3.5, the resulting equation for the first-order property can be simplified using the Hellmann-Feynman theorem: for a fully optimized wave function, the first derivative of the energy with respect to an external perturbation is equal to the expectation value of the first derivative of the Hamiltonian with respect to the perturbation.

$$\frac{\partial E}{\partial \lambda} = \frac{\partial}{\partial \lambda} \left\langle \Psi \left| \hat{H} \right| \Psi \right\rangle = \left\langle \Psi \left| \frac{\partial \hat{H}}{\partial \lambda} \right| \Psi \right\rangle \tag{3.6}$$

To evaluate a second-order property, such as the nuclear magnetic shielding tensor and the magnetically induced densities of a molecule, the second derivative of the energy can be obtained as

$$\frac{d^2 E(\lambda)}{d\lambda^2} = \left.\frac{\partial^2 E(\lambda; c)}{\partial \lambda^2}\right|_{c=c'} + \left.\frac{\partial^2 E(\lambda; c)}{\partial \lambda \partial c}\right|_{c=c'} \frac{\partial c}{\partial \lambda} \tag{3.7}$$

The last term in Eq. 3.7 can be obtained by differentiating Eq. 3.5 with respect to λ and applying the chain rule

$$\left[\frac{d}{d\lambda}\frac{\partial E(\lambda; c)}{\partial c}\right]\Bigg|_{c=c'} = \left.\frac{\partial^2 E(\lambda; c)}{\partial \lambda \partial c}\right|_{c=c'} + \left.\frac{\partial^2 E(\lambda; c)}{\partial c^2}\right|_{c=c'} \frac{\partial c}{\partial \lambda} = 0 \tag{3.8}$$

Take CC as an example of non-variational approaches, a similar relation can be obtained using the Lagrangian formulation of the response equation making the CC energy variational [81] . The response contributions ensure that the wave function is stationary to first-order in the presence of the perturbation. By introducing the following notations for the electronic gradient $F = \left.\frac{\partial E(\lambda;c)}{\partial c}\right|_{c=c'}$ and for the corresponding Hessian $G = \left.\frac{\partial^2 E(\lambda;c)}{\partial c^2}\right|_{c=c'}$, Eq. 3.8 can be written as

$$G\frac{\partial c}{\partial \lambda} = -\frac{\partial F(\lambda)}{\partial \lambda}, \tag{3.9}$$

which is called Newton's equation. The first-order response of the wave function $\frac{\partial c}{\partial \lambda}$ is obtained by solving Newton's equation. The calculation of the second-order properties needs the solution of response equation. In general, to compute energy derivatives of order $(2n+1)$ requires derivatives of variationally determined coefficients of n .

3.2 Magnetic Properties

The construction of the Hamiltonian for a molecule in the presence of a magnetic field will be introduced first. Then I will discuss a few magnetic properties which have been used as an aromaticity index for assessing the degree of molecular aromaticity.

THE HAMILTONIAN AND ITS ENERGY EXPRESSION

For molecules exposed to a uniform magnetic field with the flux density $\mathbf{B}$, the perturbation Hamiltonian for a closed-shell molecule can be derived by introducing the vector potential which describes the magnetic field [47]. The simplest way to construct the Hamiltonian in the presence of the magnetic field is to begin with the Hamiltonian in the absence of the field. The momentum $\mathbf{p}$ is then replaced by the generalized momentum $\mathbf{p} + \frac{e}{c}\mathbf{A}$ wherever $\mathbf{p}$ occurs in the Hamiltonian. The vector potential of the field $\mathbf{A}$ consists of $\mathbf{A}_{\text{ex}}$ and $\mathbf{A}_{\text{nuc}}$. The subscript "ex" denotes an externally applied field and the "nuc" describes the magnetic field arising from magnetic moment of the nucleus. The vector potential $\mathbf{A}_{\text{ex}}$ and the flux density $\mathbf{B}$ are related through $\mathbf{A}_{\text{ex}} = \frac{1}{2}\mathbf{B} \times \mathbf{r}$ whereas the vector potential $\mathbf{A}_{\text{nuc}}$ arising from the magnetic moment of the nucleus is given by $\mathbf{A}_{\text{nuc}} = \sum_I \mathbf{m}_I \times \frac{\mathbf{r}_I}{|\mathbf{r}_I|^3}$. $\mathbf{m}_I$ is the magnetic moment of the nucleus I and $\mathbf{r}_I$ denotes the position vector from the nucleus.

When the Coulomb gauge is used, the Hamiltonian for an electron in the presence of the field becomes

$$H = H^{(0)} + \underbrace{\frac{e}{cm_e}\mathbf{A}_{\text{ex}} \cdot \mathbf{p}}_{H_{\text{ex}}^{(1)}} + \underbrace{\frac{e^2}{2c^2 m_e}\mathbf{A}_{\text{ex}}^2}_{H_{\text{ex}}^{(2)}} + \underbrace{\frac{e}{cm_e}\mathbf{A}_{\text{nuc}} \cdot \mathbf{p} + \frac{e}{cm_e}\mathbf{A}_{\text{ex}} \cdot \mathbf{A}_{\text{nuc}} + \frac{e^2}{2c^2 m_e}\mathbf{A}_{\text{nuc}}^2}_{H_{\text{nuc}}} \tag{3.10}$$

The total energy of the molecular system, calculated as the expectation value of the Hamiltonian, depends now on the strength of the external magnetic field and the size of magnetic moments of the nuclei. Considering the vector potential as perturbations to the system, the energy can be expressed as a similar power series expansion as given in Eq. 3.1.

In the presence of an external magnetic field and the magnetic moments of nuclei, the total energy to the perturbed Hamiltonian can then be written as

$$E = E_0 + \frac{1}{2}\mathbf{B}^{\mathrm{T}} \underbrace{\left(\frac{\partial^2 E}{\partial \mathbf{B} \partial \mathbf{B}}\right)}_{\chi^{\mathbf{B}}} \mathbf{B} + \sum_I \mathbf{B}^{\mathrm{T}} \underbrace{\left(\frac{\partial^2 E}{\partial \mathbf{B} \partial \mathbf{m}_I}\right)}_{\sigma^I} \mathbf{m}_I + \frac{1}{2}\sum_{I,J} \mathbf{m}_I^{\mathrm{T}} \underbrace{\left(\frac{\partial^2 E}{\partial \mathbf{m}_I \partial \mathbf{m}_J}\right)}_{\sigma^{I,J}} \mathbf{m}_J \tag{3.11}$$

where the term $\chi^{\mathbf{B}}$, depending quadratically on $\mathbf{B}$, is the magnetizability tensor. The first-order linear terms in $\mathbf{B}$ and $\mathbf{m}_I$ vanish for the closed-shell molecules. The third term in Eq. 3.11 is the second-order interaction energy due to the interaction of nuclear moments with the external field; the derivative denoted σ^I is the magnetic shielding tensor of the nuclei I. The last term in Eq. 3.11 contains the spin-spin coupling of the nuclear magnetic moments.

THE NUCLEAR MAGNETIC SHIELDING

The most interesting magnetic properties of molecules are based on the parameters encountered in magnetic resonance. The parameters, including shielding constants and g-values, are related to various molecular characteristics and can be rationalized in terms of the current induced in the electronic distributions of molecules by the magnetic interaction.

Different nuclei in a molecule have different resonance frequencies since they experience differing local magnetic fields $\mathbf{B}_{\text{loc}}$ which can be related to the applied external field through $\mathbf{B}_{\text{loc}} = \mathbf{B} - \sigma\mathbf{B}$ where σ is the magnetic shielding tensor [47].

The second-order energy for the magnetic interaction between the applied field and the nuclear magnetic moment can also be expressed in terms of the induced current and the magnetic vector potential due to the corresponding nuclear magnetic moment:

$$E^{(2)}_{\mathbf{B},\mathbf{m}_I} = -\int \mathbf{A}_{\text{nuc}} \cdot \mathbf{J}^{\mathbf{B}}(\mathbf{r}) d\mathbf{r} \tag{3.12}$$

It shows how energy shifts arise from the coupling of the magnetic dipole with the currents that are induced in the electron distribution.

The magnetic shielding tensor of the nuclei I, σ^I, is the second-order change of the energy with respect to magnetic moments of the nuclei and the external magnetic field. In the limit of zero magnetic field, the magnetic shielding tensor can be obtained as $\sigma^I_{\alpha\beta} = \left.\frac{\partial^2 E}{\partial \mathbf{m}^I_\alpha \partial \mathbf{B}_\beta}\right|_{\substack{\mathbf{B}=0 \\ \mathbf{m}_I=0}}$. Differentiating the energy in Eq. 3.12 yields an alternative expression for the magnetic shielding tensor.

$$\sigma^I_{\alpha\beta} = -\varepsilon_{\alpha\delta\gamma} \int \frac{\mathbf{r}_{I\delta}}{|\mathbf{r}_I|^3} \frac{\partial \mathbf{J}_\gamma(\mathbf{r})}{\partial \mathbf{B}_\beta} d\mathbf{r} = -\varepsilon_{\alpha\delta\gamma} \int \frac{\mathbf{r}_{I\delta}}{|\mathbf{r}_I|^3} \mathbf{J}^{\mathbf{B}_\beta}_\gamma(\mathbf{r}) d\mathbf{r} \tag{3.13}$$

In Eq. 3.13, $\mathbf{J}^{\mathbf{B}_\beta}_\gamma$ are the tensor elements of the first-order induced current density, and $\varepsilon_{\alpha\delta\gamma}$ is the Levi-Civita tensor.

THE CURRENT DENSITY

More insights into the nature of magnetic properties of a molecule can be obtained by investigating the electronic currents which are induced by the applied magnetic field. Here, the current density, $\mathbf{J}(\mathbf{r},\mathbf{t})$, is introduced by differentiating the time-dependent probability density, $\rho(\mathbf{r},\mathbf{t})$, with respect to the time coordinate: $\frac{\partial}{\partial \mathbf{t}}\rho(\mathbf{r},\mathbf{t}) = -\nabla \mathbf{J}(\mathbf{r},\mathbf{t})$ which represents the charge conservation law. A change in the density in some region must be balanced by a flux in or out of that region. Therefore, the current density or the probability current can be obtained as $\mathbf{J}(\mathbf{r},\mathbf{t}) = \frac{1}{2i}\int d\mathbf{r}_2 \ldots d\mathbf{r}_N \left(\Psi^* \nabla \Psi - \nabla \Psi^* \Psi\right)$. The current must vanish when the wave function is real and when the system is independent of time. In the presence of a uniform and time-independent magnetic field introduced by the magnetic vector potential, the probability current is given by

$$\mathbf{J}(\mathbf{r},\mathbf{t}) = \frac{1}{2i}\int d\mathbf{r}_2 \ldots d\mathbf{r}_N \left(\Psi^* \nabla \Psi - \nabla \Psi^* \Psi + \frac{2i}{c}\mathbf{A}\Psi^*\Psi\right) \tag{3.14}$$

The electronic density is involved in the last term of Eq. 3.14. The other two terms are no longer zero because the wave function is distorted by the applied field. Finally, when carrying out the perturbation expansion to the first-order in the magnetic field, $\mathbf{B}$, the wave function can be expressed as $\Psi = \Psi_0 + \frac{\partial \Psi_0}{\partial \mathbf{B}}\mathbf{B} + \ldots$. Eq. 3.14 can then be written as

$$\mathbf{J}(\mathbf{r},\mathbf{t}) = \frac{1}{2i}\int d\mathbf{r}_2 \ldots d\mathbf{r}_N \left[\left(\Psi_0^{(1)*}\nabla\Psi_0 + \Psi_0^*\nabla\Psi_0^{(1)} - \Psi_0^{(1)}\nabla\Psi_0^* - \Psi_0\nabla\Psi_0^{(1)*}\right)\mathbf{B} + \frac{2i}{c}\mathbf{A}\Psi_0^*\Psi_0\right] \tag{3.15}$$

The current density can naturally be divided into two parts [48]: The last term in Eq. 3.15 is referred to as the diamagnetic current density which only depends on the ground-state wave function. The other terms are known as the paramagnetic current density depending on the admixture of excited states. However, one should keep in mind that the division of the

current density is affected by the particular choice of the gauge of the vector potential. Only the overall current density has real physical significance since both the size and the sign of two contributions vary with the selection of the gauge. For a molecule in a stationary state, the charge conservation must hold in any point of space. It can alternatively be stated in the terms of the Sambe-Epstein integral condition: $\int \mathbf{J}(\mathbf{r},\mathbf{t}) \cdot d\mathbf{r} = 0$ [32]. The currents sustained in a molecule cause a secondary magnetic field. By applying Biot-Savart's law, the strength of the induced magnetic field at nucleus I can be obtained as $\mathbf{B}_{\text{int}} = -\frac{\partial^2 E}{\partial \mathbf{m}_I \partial \mathbf{B}}\mathbf{B} = -\sigma^I \mathbf{B}$ which also defines the nuclear magnetic shielding tensor for nucleus I, σ^I.

THE USE OF GAUGE-INCLUDING ATOMIC ORBITALS

The gauge problem results from the fact that there are an infinite number of vector potentials describing a certain magnetic field, since the magnetic field is defined as $\mathbf{B} = \nabla \times \mathbf{A}$ and the gradient of any scalar function $\nabla\mathbf{\Lambda}$ can be added to $\mathbf{A}$ without changing $\mathbf{B}$. The energy of a given system must be invariant to the choice of the gauge. A transformation of the Hamiltonian by a unitary gauge transformation of the vector potential must leave the energy invariant; it can be obtained as $H(\mathbf{A}') = e^{-i\Lambda} H(\mathbf{A}) e^{i\Lambda}$ when applying a gauge transformation of the vector potential by adding the gradient of a scalar function to the vector potential $\mathbf{A}(\mathbf{r}) \rightarrow \mathbf{A}'(\mathbf{r}) = \mathbf{A}(\mathbf{r}) + \nabla\mathbf{\Lambda}(\mathbf{r})$. The corresponding wave function is related to the original wave function by a phase factor: $\Psi(\mathbf{A}') = e^{-i\Lambda}\Psi(\mathbf{A})$. The charge conservation must be fulfilled and it can be shown to be equivalent to gauge invariance by using the hypervirial theorem [82]:$\langle \Psi(\mathbf{A}) \,|[\Lambda, H(\mathbf{A})]|\, \Psi(\mathbf{A})\rangle = 0$. The exact solutions to the Schrödinger equation are gauge invariant [83], whereas approximate solutions using finite basis sets are in general not. In addition, for non-variational methods, the hypervirial theorem is not exactly satisfied [84]. However, the gauge error arising from the truncation of the basis sets is much greater than the gauge error originating from the hyperviral theorem problems of non-variational methods.

To deal with the gauge problem, London proposed to use explicitly field-dependent basis functions [85]. The basis functions are defined as

$$\chi_\mu(\mathbf{r}) = e^{-\frac{i}{2c}(\mathbf{B}\times[\mathbf{R}_\mu - \mathbf{R}_o]\cdot\mathbf{r})}\chi^0_\mu(\mathbf{r}) \tag{3.16}$$

where $\chi^0_\mu(\mathbf{r})$ denotes a standard magnetic field independent basis function with $\mathbf{R}_\mu$ as center and $\mathbf{R}_o$ is the chosen gauge origin. They are called either London orbitals or Gauge-Including Atomic Orbitals (GIAOs). The use of GIAOs eliminates the explicit reference to the global gauge origin $\mathbf{R}_o$ in the expressions for the nuclear magnetic shielding constants [86]. Furthermore, it ensures a rapid basis set convergence for many second-order magnetic properties. One should be aware that the GIAOs are not proper gauge transformations of either the wave function or the molecular orbitals. Gauge invariance is not achieved by using them, whereas gauge independence is though obtained. Within the GIAO framework, Wolinski *et al.* introduced modern analytic derivative theory to efficiently calculate the nuclear magnetic shieldings [87]. Since then, the GIAO approach has been implemented any many levels of theory in most quantum chemistry program packages.

3.3 The Magnetic Criteria for Aromaticity

Since Faraday isolated benzene from the liquid residue formed during the production of lamp gas in 1825, the concept of aromaticity constitutes a fundamental topic and lies at the

heart of chemistry [32]. There are ca. 300000 papers dealing with the aromatic properties of chemical systems published in the scientific literature since 1981 [88]. In modern organic chemistry textbooks, aromatic compounds are considered as having high stability. They have an exceptional chemical behavior for highly unsaturated structures with a tendency to undergo ionic substitution. Several attempts have been made to define and quantify the aromatic characters of substances; in particular, theoreticians have introduced a number of suitable indices to be used as computational measures of aromaticity. In this section, I shall discuss a few of them.

MAGNETIC SUSCEPTIBILITY ANISOTROPY

Exalted magnetic susceptibilities, Λ, were the first magnetic criterion to be employed to characterize aromaticity. They represent the variation of diamagnetism due to the molecular conjugation [89]. It was understood that the enhanced diamagnetic aromaticity is related to the fully delocalized electrons sustaining ring currents. Based on comparisons of theoretical and experimental degrees of aromaticity for a series of aromatic molecules, it was pointed out by many researchers that one cannot expect agreement between the calculated London or ring-current diamagnetism and the magnetic anisotropy because the important paramagnetic contribution to the anisotropy is not included [30, 90, 91].

If a sample of anisotropic molecules is exposed to a magnetic field, the molecule tends to orient itself in such a way that the axis of maximum algebraic susceptibility in the rotation plane approaches the direction of the lines of the force. For example, a small alignment of benzene has been experimentally observed [92]. Flygare and his coworkers were entirely aware of the importance of experimental studies and developed the general concept of magnetism in aromatic systems [93, 94, 95, 96]. By studying the Zeeman effect in microwave spectra, they gave an outstanding contribution to measurement and rationalization of molecular magnetic response properties of a great number of compounds. They considered the values of the susceptibility anisotropy $\Delta\chi = \chi_{zz} - \frac{1}{2}(\chi_{xx} + \chi_{yy})$ as a criterion of aromaticity or delocalization of π–electrons in ring systems. The $\Delta\chi$ value is the out-of-plane susceptibility component minus the average in-plane components of the susceptibility tensor. From the experimental point of view, this criteria provided a fundamental tool for the assessment of RCM [97].

CHEMICAL SHIFTS

The calculations for NMR shieldings at various levels of theory have been developed to be a standard tool in chemistry [98, 99, 100] since NMR spectroscopy is considered as one of the best analytical methods for characterizing molecular structures [101]. Magnetically active nuclei, such as ^{1}H and ^{7}Li, can be used to probe the nearby shielding influences because of the sensitivities to the electronic structures. ^{1}H and ^{7}Li NMR chemical shifts can be also used to demonstrate aromaticity. The chemical shifts of hydrogens in bridging positions have been used to provide the examinations of aromaticity and antiaromaticity because the rings of most aromatic systems are too small to adapt inner protons [102]. Because the lithium bonding is electrostatic, experimental ^{7}Li chemical shifts generally show little variation among different compounds. In general, lithium cations complex at the π faces of aromatic systems exhibiting significant shielding or deshielding of the ^{7}Li NMR signals and the ^{7}Li chemical shifts can be used to examine induced ring current effects. However, the distances between Li^+ and the aromatic rings are at least 2 Å so the ring current effects are relatively small. The number of Li^+ complexes is limited; therefore, it narrows the utility of Li^+ as an aromaticity probe.

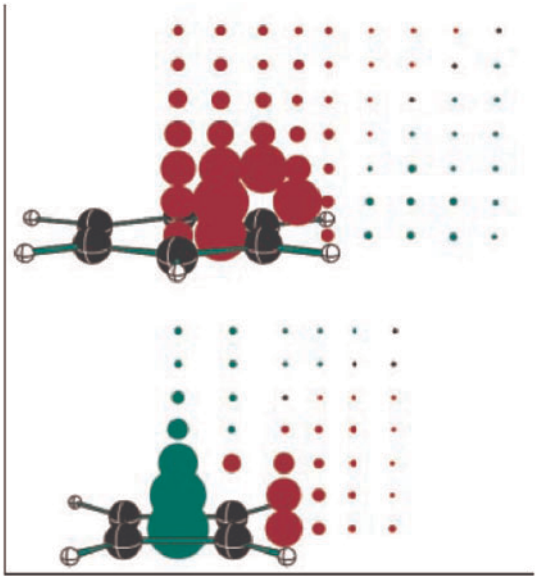

Figure 3.1: The NICS grid plot of benzene and cyclobutadiene calculated at the GIAO-B3LYP/6-311+G*//B3LYP/6-311+G* level of theory. The red and green dots denote diatropic (aromatic) and paratropic (antiaromatic) ring currents, respectively [103].

NUCLEUS-INDEPENDENT CHEMICAL SHIFT

The nucleus-independent chemical shifts (NICS) introduced by Schleyer *et al* in 1996 are used to probe aromaticity by computing the absolute chemical shielding at any point of space [26]. The development of NICS emanated from studies of ring current effects on the chemical shifts of ^{1}H and Li^{+} above aromatic rings. They were aware of the fact that H and Li probe nuclei would not only measure the magnetic shielding in that point but they also affect the outcome of the calculations. However, the magnetic shielding can also be computationally measured by using virtual or dummy atoms as probes and thus avoiding the modifications of the sample.

NICS indices correspond to the negative magnetic shielding computed at chosen points in the vicinity of molecules. They are typically calculated at the centers of rings and cages, at points above the molecular rings, and even in uniformly distributed grid points yielding complete magnetic shielding functions. The grid distribution of NICS values illustrated for C_4H_4 and C_6H_6 is shown in Figure 3.3 [103]. Large negative NICS values calculated in the interior positions of rings and cages indicate the presence of induced diatropic ring currents and aromaticity, whereas positive values denote paratropic ring currents and antiaromaticity. There are several reasons why this very simple method has recently become a popular tool for assessing molecular aromaticity: (i) No reference standards, increment schemes, nor calibrating equations for evaluation are required. (ii) In contrast to exalted magnetic susceptibilities, which depend on the square of the ring area, NICS only shows the dependence on the ring size and the number of π electrons. (iii) NICS correlates well with other aromaticity indices based on energetic, geometric and magnetic criteria [88, 104, 105, 106, 107].(iv) It is easy to compute NICS by using standard quantum chemical programs.

Usually NICS gives qualitative agreement with other aromaticity indices; however, a number of studies have risen the question: can NICS really be used to detect ring currents, and

does it yield a quantitative index of aromaticity [32, 108, 109, 110]. The reasons why NICS in general is not a reliable descriptor of aromaticity have been explained by Lazzeretti [111]. NICS is calculated as one third of the negative trace of the shielding tensors at the center of the ring. The trace is the sum of the three diagonal components whose relative magnitudes may be very different from each other. Therefore, the information about the out-of-plane deshielding, which is the unique possible measure of magnetic aromaticity, is unavoidably lost in the average NICS. More reliable aromaticity indices would possibly be obtained from the out-of-plane component of the shielding tensor, or alternatively the anisotropy of the shielding defined as the out-of-plane minus average in-plane components.

Above all, NICS works so far pretty well for simple aromatic systems, such as benzene; however, it fails to describe or predict the aromaticity properties for more complicated systems such as the copper clusters with Cu_4^{2-} rings which were studied in this work.

AROMATIC RING-CURRENT SHIELDINGS

The Aromatic Ring-Current Shieldings (ARCS) method was developed by Jusélius *et al.* [112] The nuclear magnetic shieldings are calculated for a set of points along a line perpendicular to the aromatic ring. The shielding as a function of distance from the center of the molecular ring $\sigma(\mathrm{r})$ is used to determine the degree of aromaticity which is often assumed to be proportional the strength of the ring current. This method is the first attempt to quantify the strength of the ring current.

The long-range shielding results from the magnetic field induced by the ring current circulating in a molecular ring. By using the Biot-Savart law [113], the long-range shielding can be related to the strength of the currents sustained in the ring. The ring current susceptibility, $\frac{\partial \mathbf{I}}{\partial \mathbf{B}_{ex}}$, can be estimated by using the expression for an infinity thin circular conducting wire

$$\sigma(\mathrm{r}) = -\frac{\mu_0}{2}\frac{\partial \mathbf{I}}{\partial \mathbf{B}_{ex}}\frac{\mathrm{R}^2}{(\mathrm{r}^2+\mathrm{R}^2)^{3/2}} \tag{3.17}$$

where μ_0 is the permeability of vacuum, R is the ring radius, and r is the perpendicular distance from the ring center. The ring current strength from a given magnetic field can be obtained as $\mathbf{I} = \frac{\partial \mathbf{I}}{\partial \mathbf{B}_{ex}}\mathbf{B}_{ex}$. The maximal r values needed in a ARCS calculation depends on the aromatic ring size. It is usually 30-60 Bohr. At short distances, the shielding function does not fit the Biot-Savart law due to local current densities and eventually the presence electron charge. Therefore, it is necessary to choose the minimal r value properly in order to get reasonable fits. However, as long as the part of the shielding function inside the electron charge distribution area is avoided, the results are quite stable.

The ARCS value is, as the NICS value, deduced from the isotropic shieldings making the ARCS method a less reliable tool for accessing the degree of aromaticity for more complicated multi-ring species. A more accurate aromaticity index might be obtained by using the perpendicular components of the shielding function in the ARCS fit.

THE GIMIC METHOD

The GIMIC method [114] applied through the studies done in this thesis is based on the ring-current model (RCM). The essential features of RCM were first outlined by Pauling [27], Lonsdale [115] and London [28, 85, 116] in an attempt to explain experimental results. For planar or nearly planar molecules, they found that the diamagnetic susceptibility of

aromatic molecules is numerically much greater in a direction normal to the ring plane than in the directions parallel to it [115]. RCM has later been refined and extended by Pople [117, 118] and McWeeny [119]: the former first interpreted the chemical shift of benzene observed in proton magnetic resonance in terms of ring current and the later successfully developed a semiempirical approach to calculate the current.

The GIMIC method to calculate magnetically induced current densities is based on analytical derivative theory and the use of GIAOs. The derivation is achieved by comparing the nuclear magnetic shielding tensor from the Biot-Savart's expression in Eq. 3.13 with the tensor given by the quantum chemistry expression for the second-order change of the energy with respect to the nuclear magnetic moment and the external magnetic field [120].

Together with the use of field-dependent basis functions $\chi_\mu(\mathbf{r})$ given in Eq. 3.16, the components of the magnetically induced current density tensor can be obtained as

$$\begin{aligned}\mathcal{J}_\alpha^{\mathbf{B}_\beta}(\mathbf{r}') &= -\varepsilon_{\alpha\beta\delta}\sum_{\mu\nu} D_{\mu\nu}\chi_\mu^*(\mathbf{r}')\frac{\partial^2\tilde{h}}{\partial\mathbf{m}_\alpha^I\partial\mathbf{B}_\delta}\chi_\nu(\mathbf{r}') + \sum_{\mu\nu}\frac{\partial D_{\mu\nu}}{\partial\mathbf{B}_\delta}\chi_\mu^*(\mathbf{r}')\frac{\partial\tilde{h}}{\partial\mathbf{m}_\alpha^I}\chi_\nu(\mathbf{r}') \\ &\quad + \sum_{\mu\nu} D_{\mu\nu}\frac{\partial\chi_\mu^*(\mathbf{r}')}{\partial\mathbf{B}_\delta}\frac{\partial\tilde{h}}{\partial\mathbf{m}_\alpha^I}\chi_\nu(\mathbf{r}') + \sum_{\mu\nu} D_{\mu\nu}\chi_\mu^*(\mathbf{r}')\frac{\partial\tilde{h}}{\partial\mathbf{m}_\alpha^I}\frac{\partial\chi_\nu(\mathbf{r}')}{\partial\mathbf{B}_\delta}\end{aligned} \tag{3.18}$$

with the derivatives of the one-electron Hamiltonian which are defined as

$$\left.\frac{\partial\hat{h}}{\partial\mathbf{m}_I}\right|_{\substack{B=0\\ \mathbf{m}^I=0}} = -\frac{i}{c}\frac{\mathbf{r}_I\times\bigtriangledown}{|\mathbf{r}_I|^3} = \frac{\left.\frac{\partial\tilde{h}}{\partial\mathbf{m}_I}\right|_{\substack{B=0\\ \mathbf{m}_I=0}}}{|\mathbf{r}_I|^3},\quad \left.\frac{\partial^2\hat{h}}{\partial\mathbf{m}_I\partial\mathbf{B}}\right|_{\substack{B=0\\ \mathbf{m}_I=0}} = \frac{1}{2c^2}\frac{(\mathbf{r}_o\cdot\mathbf{r}_I)\,\mathbf{1}-\mathbf{r}_o\mathbf{r}_I}{|\mathbf{r}_I|^3} = \frac{\left.\frac{\partial^2\tilde{h}}{\partial\mathbf{m}_I\partial\mathbf{B}}\right|_{\substack{B=0\\ \mathbf{m}_I=0}}}{|\mathbf{r}_I|^3} \tag{3.19}$$

The resulting expression in Eq. 3.18 only involves basis functions and the derivatives of basis functions in discrete points as well as the corresponding one-electron density matrices, and it is easily evaluated at any point in space except at the nuclei. The singularity at the nuclei can be avoided because the same denominator $|\mathbf{r}_I|^3$ occurs in every term of Eq. 3.18. Even though the second-order derivatives of one-electron Hamiltonian is explicitly dependent on the gauge origin seeming to make the current tensor gauge dependent, it can be shown that the gauge-dependent terms cancel exactly with the terms arising from the differentiation of the GIAOs. Therefore, no reference to the gauge origin appears in the final expression for the first-order induced current density. As discussed previously, the obtained currents are gauge-origin independent but not gauge invariant. The gauge invariance is only acquired in the limit of a complete basis set, and the gauge problem leads to non-zero divergence [114].

The use of GIAOs yields gauge-independent current densities with a fast basis-set convergence; standard basis sets give current densities close to the basis-set limit making GIMIC calculations on large molecules feasible. GIMIC calculations can also be performed at any computational level for which the one-body density matrix and the magnetically perturbed density matrices are available. This method is hence an important tool in our studies.

Chapter 4

Results

SEVERAL molecular systems have been studied by applying the methods described in the previous chapters. We first paid attention on the lithium-aluminum clusters with composition of $LiAl_4^-$, Li_2Al_4, $Li_3Al_4^-$ and Li_4Al_4. Even though many studies on these clusters had been carried by other groups [121, 122, 123], the details of aromatic properties were not well clarified. In this work, the aromatic properties of the Al_4^{2-} and Al_4^{4-} cores were accessed computationally by employing different aromaticity indices. It showed that the GIMIC method is a useful tool for analyzing the nature of aromaticity for these clusters. The GIMIC applications were then extented to some copper clusters based on the idea of planar copper rings proposed by Tsipis, Fuentealba, and Chen [124, 125, 126, 88]. Our collaborators, Wang *et al.*, were able to produce the Cu_4Na^-, Au_4Na^- and other small sodium-auride clusters at that time; they further characterized these clusters by photoelectron spectroscopy[2]. The computationally simulated PES spectra were used to identify the molecular structure of these two clusters observed in the PES experiment. The calculations were carried out at the CCSD level using the equation-of-motion coupled-cluster (EOMIP) approach. In order to understand the electron delocalization and aromaticity properties of the Cu_4^{2-} ring, the magnetically induced current densities calculated for Cu_4Li^- and Cu_4Li_2 using the GIMIC method. The ring-current strengths and the shape of the ring current clearly demonstrated that the square-shaped planar Cu_4^{2-} four-membered rings are σ-aromatic systems primarily due to the *s* orbital bonding.

Many bimetallic sodium auride clusters have experimentally been studied since the first observation of diatomic NaAu 30 years ago [15, 17, 127, 128, 129, 130]. The generation of small anionic sodium-auride clusters with the composition of $Na_mAu_n^-$ ($n = 1-4, n \geq m$ and $m+n \leq 6$) was recently reported [2, 4]. The structures of the anionic clusters were also determined by comparing experimental and computational photoelectron spectra (PES). The calculations showed that the clusters have many low-lying isomers making an identification difficult based on calculations. However, the computed PES spectra of the isomers significantly differ rendering the structure determination feasible when having access to experimentally measured spectra. Explicit calculations of the electron density showed that the excess electron of the anions is basically shared by the gold atoms yielding a preference for the formation of extended cluster structures with separated gold atoms to minimize the Coulomb repulsion.

Table 4.1: The analysis of the vibrational frequency calculations of benzene acquired at the MP2 level by employing different basis sets.

	At least one vibrational frequency	All frequencies are real
Uncontraction basis sets [a]	12S6P/5S, 12S6P1D/5S[b], 12S6P/6S, 12S6P1D/6S[b]	12S6P2D/5S[c], 12S6P2D1F/5S[c], 12S6P2D/6S[c], 12S6P2D1F/6S[c]
contracted basis sets	6-311+G, 6-311+G(d), 6-311+G(d,p), 6-311++G 6-311++G(d)	6-311+G (2d), 6-311+G (2df), 6-311+G (2d, p), 6-311+G (2df,p), 6-311++G (2d) 6-311++G (2df)

a. Even-tempered basis sets
b. D function is extracted from the Dunning cc-pVDZ basis set
c. D and F functions are extracted from the Dunning cc-pVTZ basis set

4.1 Molecular Structures

Finding a proper minimum structure is the first step of examining a molecular system. In our cases, the lithium-aluminum clusters were optimized at the CCSD level while the molecular structures of other clusters were obtained at the RI-MP2 level which is the most applicable *ab initio* method. In our studies, the MP2 method indeed provides valuable information. Instead of reviewing the molecular structures obtained in the MP2 optimization, I shall simply discuss how the MP2 method works and some problems we found. The optimized structures are discussed in the enclosed publications.

THE MOLECULAR STRUCTURE OF BENZENE AND $Na_2Au_3^-$

It has been recently discovered that the post-HF methods such as MP2 in conjunction with standard basis sets might predict the benzene structure to be non-planar [131]. In Table 4.1, it shows that the planar benzene was obtained only with the higher angular momentum function introduced for both contracted and uncontracted basis sets. The deficiency in MP2 method occurs until a better description of the Coulomb correlation can be provided with the use of large enough basis sets.

Also, the structural information obtained at the MP2 and DFT levels is known to be distinct for small gold clusters; therefore, the choice of appropriate basis sets for the molecules should be carried out with care. For the $Na_2Au_3^-$ anion, the two lowest isomers at the MP2/QZVPP level is a linear cluster (Figure 4.1a) and a planar conformation of C_s symmetry (Figure 4.1b). The linear isomer is the lowest structure at the MP2/QZVPP level, whereas the planar one is a local minimum only 6 kJ/mol higher in energy; in single-point SCS MP2/QZVPP calculations, the linear $Na_2Au_3^-$ isomer is 30 kJ/mol below the planar one. The linear isomer is also observed in the experiment. Optimization of the cluster structures for $Na_2Au_3^-$ using the TZVPP and QZVPP basis sets yielded significantly different geometries. At the MP2/TZVPP level, a bent structure of C_{2v} symmetry (Figure 4.2) was obtained, whereas at the MP2/QZVPP level the corresponding minimum is the linear structure. The bent $Na_2Au_3^-$ structure is found probably due to the two-electron basis-set incompleteness error also found to result in nonplanar benzene at *ab initio* correlation levels

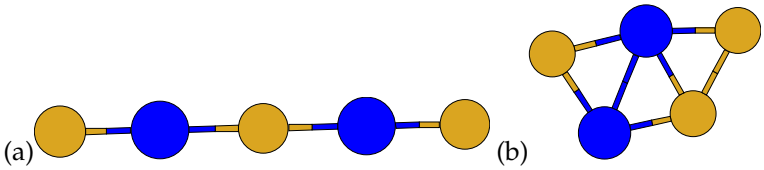

Figure 4.1: The molecular structures of $Na_2Au_3^-$ obtained at the MP2/QZVPP level: (a) a linear structure and (b) a planar conformation of C_s symmetry.

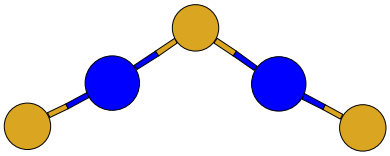

Figure 4.2: The molecular structure of $Na_2Au_3^-$ obtained at the MP2/TZVPP level: a bent structure of C_{2v} symmetry

when too small basis sets are employed [131]. The two-electron basis-set incompleteness error can make bent structures artificially lower in energy than planar and linear clusters.

4.2 Photoelectron Spectrum Studies

Photoelectron spectroscopy utilizes photo-ionization and energy-dispersive analysis of the emitted photoelectrons to study the composition and electronic state of molecules. The photoelectron spectrum can be experimentally obtained as follows [132]: The clusters are first produced by laser vaporization of targets; after each cluster is possessed of an additional electron, the anions are extracted from the cold cluster beam perpendicularly and separated by a time-of-flight mass spectrometer. The cluster anions of interest were then selected and decelerated before crossing with a detachment laser beam in the interaction zone of the magnetic-bottle PES analyzer. Finally, photoelectrons were collected by the magnetic-bottle and analyzed in a long electron flight tube. The computed photoelectron spectra can be achieved either by performing the ionization-potentials calculation of the cluster anion using the EOM-IP or alternatively by calculating the energy difference between the anion and the neutral of the cluster and adding the excitation energy of the neutral system. In the calculations of excitation energies, the optimized anion structure should be used. In our studies, the ionization potentials using EOM-IP approach were obtained at the CCSD level, and the excitation energies were calculated at the RI-CC2 level. In the alternative and more accurate approach, the first ionization potential (IP) was calculate as the MP2 energy difference between the anionic and the neutral clusters. The energetically higher PES transitions were acquired by adding the lower excitation energies of the neutral system to the first IP. It will be followed by an example of the comparison between experimental and computational PES.

THE EXPERIMENTAL AND COMPUTATIONAL PHOTOELECTRON SPECTRA: THE $NaCu_4^-$ AND $NaAu_4^-$ CLUSTERS.

The combination of photoelectron spectroscopy (PES) and computational chemistry calculations provides information of the character of the molecular structure and its electronic

Table 4.2: The vertical detachment energies (VDE in eV) for $LiCu_4^-$, $NaCu_4^-$, and $NaAu_4^-$ calculated at the EOMIP-CCSD level as compared to the experimental data.

$LiCu_4^-$	$NaCu_4^-$			$NaAu_4^-$		
calcd	calcd		exp	calcd		exp
(C_{4v})	(C_{4v})	(C_{2v})		(C_{4v})	(C_{2v})	
1.313	1.229	1.137	1.13	2.501	2.662	2.98
3.193	3.259	2.586	3.26	3.769	3.980	4.12
3.636	3.864	3.840	3.84	4.295	4.751	4.79
4.062	3.876	3.871		4.923	4.758	4.98

states, and it can be used to determine the molecular structure. It is especially useful to apply this approach for the energetically lower isomer structures of a cluster when the energy differences between these isomers are small.

The molecular structures of the C_{4v} and C_{2v} symmetries are the two energetically lowest isomers of the anionic sodium-metal coinage-metal clusters (NaM_4^-, M=Cu, Ag, and Au) obtained at the MP2 level, and the relative energies were calculated at the MP2, CCSD, CCSD(T) levels. Even if the higher correlated methods with adequate basis sets were introduced, finding the global minima of the molecular structures for these clusters is still challenging. The vertical detachment energies (VDE) calculated at the EOMIP-CCSD level for $LiCu_4^-$, $NaCu_4^-$, and $NaAu_4^-$ as well as the experimental data for $NaCu_4^-$, and $NaAu_4^-$ are listed in Table 4.2. The PES patterns of the two isomers for $NaCu_4^-$ as well as for $NaAu_4^-$ are quite different since the distinctive PES feature results from the character of the electronic states of each system. It can be seen in Table 4.2 that the computational PES of the C_{4v} isomer for $NaCu_4^-$ and the C_{2v} isomer for $NaAu_4^-$ agree well with the corresponding experimental PES spectra indicating that the observed structures of $NaCu_4^-$ and $NaAu_4^-$ are the pyramidal structure of C_{4v} symmetry and the C_{2v} planar conformation, respectively [2]. This is an example illustrating that both the experimental PES and the corresponding calculations are of vital importance in cluster identification. In addition, the similarity of the computational PES spectra of the $LiCu_4^-$ and the $NaCu_4^-$ clusters suggests the stability of the Cu_4^{2-} core in these two clusters and the role of Li and Na atoms as a supporting cation.

4.3 The aromaticity of Al_4^{2-}, Al_4^{4-}, Cu_4^{2-} and $(HF)_3$

In this section, the discussion starts with the aromaticity related calculations for the clusters consisting of all-metal four-membered rings. By applying the GIMIC method, the strong diatropic currents sustain mainly by the σ orbitals in all clusters. The Al_4^{2-} ring in $LiAl_4^-$ and Li_2Al_4 is found to also have substantial π aromaticity, the Al_4^{4-} moiety in $Li_3Al_4^-$ and Li_4Al_4 contrarily π antiaromaticity, whereas no evident currents were noticed in π-orbital region of the Cu_4^{2-} species [1, 2].

Table 4.3: The integrated ring-current susceptibilities (in nA/T) for $LiAl_4^-$, Li_2Al_4, $Li_3Al_4^-$, Li_4Al_4, $LiCu_4^-$ and Li_2Cu_4 calculated at the CCSD level using the GIMIC method

	$LiAl_4^-$	Li_2Al_4	$Li_3Al_4^{-b}$	Li_4Al_4	$LiCu_4^-$	Li_2Cu_4	Cu_4H_4
diamagnetic	32.4	36.7	18.9	18.6	19.4	23.2	2.1
paramagnetic	0.0	0.0	-19.9	-16.8	-0.4	-0.4	-2.7
total current	32.4	36.7	-1.0	1.8	19.0	22.8	-0.6
contributed by Li[a]	4.3	8.6	4.9	4.9	6.4	12.9	—
total ring current	28.1	28.1	-5.9	-3.1	12.6	10.0	-0.6

[a]The estimated net current circling around the Li+ cations.
[b] The currents passing the two identical Al-Al bonds are given in the table. The corresponding values for the shortest Al-Al bond are 22.4, -23.6, -1.3, 4.9 and -6.2 nA/T, respectively.

ALL-METAL FOUR-MEMBERED RINGS: Al_4^{2-}, Al_4^{4-} and Cu_4^{2-}

The first-order magnetically induced current densities for the Al_4^{2-}, Al_4^{4-} and Cu_4^{2-} compounds were calculated at the CCSD level using the GIMIC method. The obtained current densities are used to provide not only qualitative but also quantitative information of the aromaticity.

The degree of aromaticity for the all-metal four-membered rings is based on the numerical integrations [120] of the current densities passing the Al-Al and Cu-Cu bonds. As an example, the molecular ring and the integration plane cutting the Al-Al bond are shown in Figure 4.3. Quantitative values for the diatropic and paratropic contributions to the ring currents can be acquired by integrating them individually *i.e.* separating the positive and negative contributions to the total current. The integrated current strengths are given in Table 4.3. The positive currents are here defined as the diatropic currents whereas the negative values denote paratropic currents. The diatropic and paratropic currents are related to aromatic and antiaromatic features, respectively. The ring-current strength circling the ring was calculated as the subtraction of the total current strengths and the induced currents circling around the Li^+ cations above the ring center. For comparison, the ring current susceptibility of benzene was found to be 11.8 nA/T calculated at the CCSD/TZP level [120]. As the net current susceptibility for Al_4^{2-} is positive, it can be considered to be an aromatic aluminum four-membered ring, whereas the small but negative current susceptibilities for the Al_4^{4-} species show that they are non-aromatic or possibly weakly antiaromatic. The integration planes cutting through different Al-Al bonds in $Li_3Al_4^-$ yield qualitatively the same current strengths. The net current susceptibilities only differ by 0.3 nA/T (5%). The ring-current susceptibility of the Cu_4^{2-} ring is about as large as in benzene and 2-3 times weaker than for the Al_4^{2-} species. The Cu_4 ring in Cu_4H_4 does not sustain any strong magnetically induced ring current. The weak diatropic current circles inside and outside the Cu_4 ring, whereas the region in the vicinity of the H atoms and outside them is dominated by a paratropic ring current. The net ring-current susceptibility for Cu_4H_4 is only -0.6 nA/T. Thus, Cu_4H_4 is not aromatic as previously suggested.

Also, the integrated current strengths are defined as a function of the radius (width) of the integration cross section, and numerical differentiation of the current function with respect to the radius (width) yields the profile of the ring currents passing the integration plane. In Figure 4.4, the contributions from σ and π orbitals were evaluated separately for the

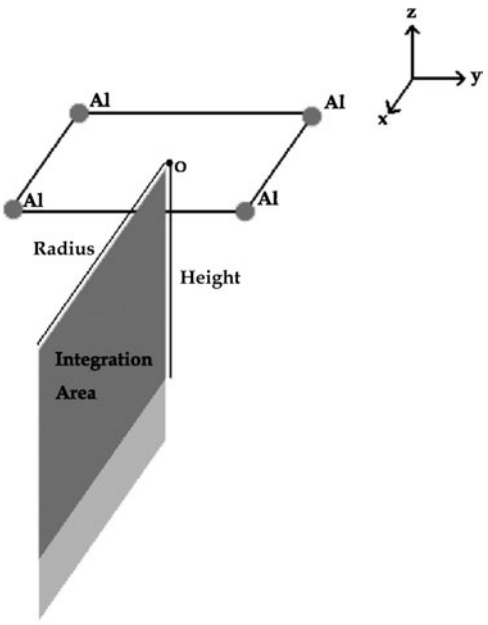

Figure 4.3: The integration cross section used in the calculation of the integrated current-density distributions.

Table 4.4: For $LiAl_4^-$, Li_2Al_4, $Li_3Al_4^-$ and Li_4Al_4, the NICS values were calculated at B3LYP/TZVP and CCSD/TZP levels using the CCSD/TZP optimized structures. (in ppm)

	$LiAl_4^-$	Li_2Al_4	$Li_3Al_4^-$	Li_4Al_4
B3LYP/TZVP	-18.2	-1.7	-5.9	-10.4
CCSD/TZP	-24.1	-6.5	-10.5	-16.7

$LiAl_4^-$ and Li_4Al_4 current-density profiles. For the Al_4^{2-} species, strong diatropic currents are sustained in both the σ and the π orbitals and the integrated ring-current contributions from these orbitals are 16.7 and 9.0 nA/T, respectively. The ring of the Al_4^{2-} species can thus be considered to be both σ and π aromatic. For Li_4Al_4, the integrated diamagnetic ring-current contributions from the σ and the π orbitals are 11.8 and 1.9 nA/T, whereas the corresponding paramagnetic contributions are -0.4 and -8.4 nA/T. $Li_3Al_4^-$ as well as Li_4Al_4 sustain significant diatropic and paratropic currents: strong paratropic currents are sustained in the π region while diatropic currents are contributed by the σ electrons.

One might claim that the Al_4^{4-} species are σ aromatic and π antiaromatic. This interpretation is also supported by the ARCS calculations. The ARCS functions show that the ring currents in the Al_4^{4-} species give rise to paramagnetic shieldings distant from the molecular ring, whereas the magnetic shielding function is positive at small distances from the ring [1]. Even though the strength of the net ring current in the Al_4^{4-} species is close to zero as shown by the GIMIC calculations, the molecule possesses a significant magnetic shielding at long distances from the Al_4 ring outside the electron density. For nonaromatic molecules, the magnetic shieldings away from the ring weakens fast and becomes practically zero outside the charge density. Therefore, the Al_4^{4-} species are neither aromatic, antiaromatic, nor nonaromatic. Instead, the Al_4^{4-} species can be considered to belong to a

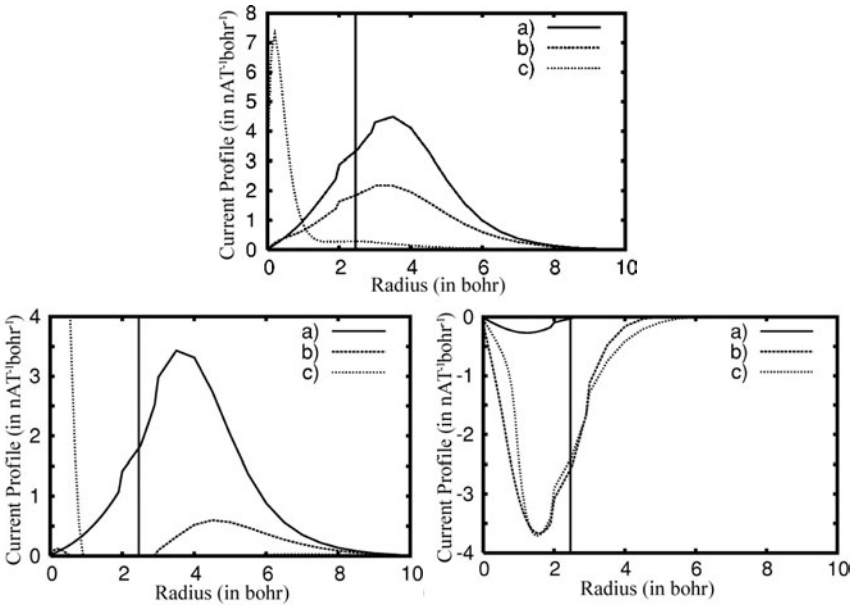

Figure 4.4: The current-density profiles for $LiAl_4^-$ and Li_4Al_4 calculated at the CCSD/TZP level: total current of $LiAl_4^-$ (upper), the diatropic current-density of Li_4Al_4 (lower left) and paratropic current-density of Li_4Al_4 (lower right). The integration intervals (in bohr) in the width direction are defined as three parts: (a) [-1.5, 1.5], (b) [-3.5, -1.5] + [1.5, 3.5], and (c) [-10.0, -3.5] + [3.5, 10.0], representing the σ density, the π density, and the rest.

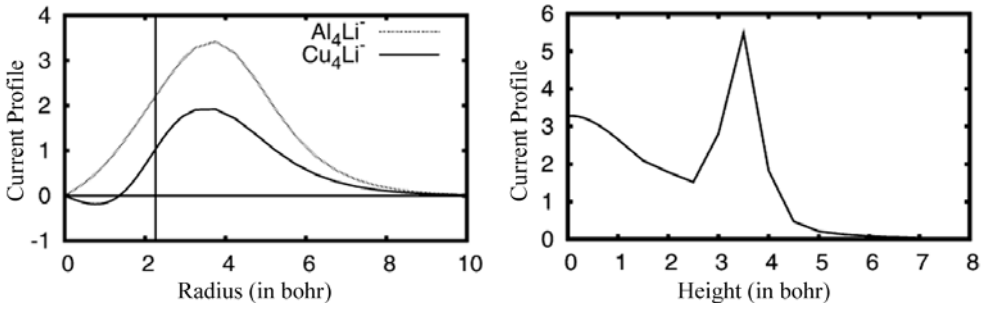

Figure 4.5: The current-density profiles calculated at the CCSD/TZVPP level as a function of the radius for $LiCu_4^-$ (left) and as a function of the height for Li_2Cu_4 (right)

new class of molecules with the peculiar property of having long-range magnetic shieldings without sustaining any strong net ring current. Another member of this class of molecules is C_{60} which has recently studied by Johansson *et al.* [133] ARCS studies show that the current in the five-membered rings is mainly paratropic and the six-membered rings sustain diatropic currents [134]. The spherical rings current is diatropic outside and paratropic inside the fullerene. For this class of molecules, the long-range magnetic shielding does not vanish, because the average radii of the diatropic and paratropic currents are significantly different. According to Biot-Savart's law, the current with the largest radius characterizes the magnetic shieldings at very long distances.

The NICS calculations for $LiAl_4^-$, Li_2Al_4, $Li_3Al_4^-$ and Li_4Al_4 were employed here for comparison. The NICS values calculated at B3LYP/TZVP and CCSD/TZP levels are also listed in Table 4.4. The negative NICS values suggest that they are all aromatic. The approximately constant difference between the NICS values calculated at the B3LYP and CCSD levels is due to the well-known fact that magnetic shieldings are in general underestimated at DFT levels of theory [135]. The number of counter ions should not significantly affect the magnitude of aromaticity properties in the aluminum four-membered-rings due to only small structural changes of the Al_4^{2-} core between $LiAl_4^-$ and Li_2Al_4. However, the NICS values of $LiAl_4^-$ do not agree with those obtained for Li_2Al_4. The NICS data for $Li_3Al_4^-$ are about 5 ppm smaller than the data for Li_4Al_4 indicating that the NICS value is not a very reliable aromaticity index for ${Al_4}^{2-}$ and ${Al_4}^{4-}$ species.

The current-density profiles calculated at the CCSD/TZVPP level as a function of the radius for $LiCu_4^-$ and as a function of the height for Li_2Cu_4 are shown in Figure 4.5. The current profiles of $LiCu_4^-$ and $LiAl_4^-$ are strikingly similar except that for Cu_4^{2-} the current in the interior of the molecular ring is weak and dominantly paramagnetic, whereas for Al_4^{2-} the ring current is diatropic both inside and outside the ring. The orbital plot in Figure 4.6 shows that the a_{1g} orbital has large amplitude at the center of the Li_2Cu_4 cluster. The presence of a significant amount of electron charge at the cluster center shields the external magnetic field in the NICS point. The diamagnetic shielding contribution from the a_{1g} orbital in the NICS point apparently results from the presence of its electrons but not from ring currents sustained in the Cu_4 ring. The e_u orbital is however ring-shaped and has a significant amplitude outside the Cu_4^{2-} ring suggesting that the HOMO is sustaining the ring current and therefore responsible for the aromaticity properties of the Cu_4^{2-} ring; in other words, the large ring current appearing outside the Cu_4^{2-} ring indicates that the e_u orbital is mainly responsible for the transport of the electrons.

The explicit orbital contributions to the magnetically induced currents cannot be obtained using the GIMIC method, because the current contributions from the mixing of occupied orbitals cannot be eliminated in the GIMIC scheme [136]. The contribution from valence 4*s* orbitals was therefore estimated by removing valence *s* functions from the basis set. In the current calculations without valence s orbitals, the ring-current susceptibility obtained at the MP2 level is only 4.0 nA/T; the Cu_4^{2-} ring sustains only a weak ring current when the valence s basis functions are absent. In contrast to Wannere et al. [88], we find no need to invoke the *d*-orbitals in order to explain the aromaticity of planar four-membered Cu_4^{2-} rings.

AROMATICITY ORIGINATED FROM THE HYDROGEN BONDS IN $(HF)_3$?

Despite the fact that aromaticity is not very well defined, new computational tools are widely used to discuss even predict molecular aromaticity qualitatively and quantitatively.

Figure 4.6: The HOMO (left) and HOMO-1 (right) molecular orbitals of Li_2Cu_4 calculated at the HF SCF/TZVPP level using the MP2/TZVPP molecular structure. The orbitals are viewed along the C_4 axis. The orbital energies (in eV) are given within parentheses. The pictures have been made using gOpenMol [137].

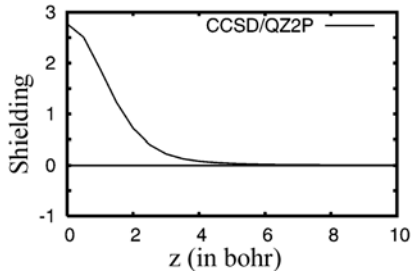

Figure 4.7: Nuclear magnetic shielding function (in ppm) of $(HF)_3$ calculated at the CCSD/QZ2P level. The shielding function is calculated from the ring center along the symmetry axis perpendicular to the ring.

As a result, new aromaticity concepts are introduced from time to time. The term H-bonded aromaticity was recently proposed by Datta et al. based on the significant diamagnetic shieldings at the center of cyclic HX (X=F, Cl, and Br) trimers and water molecules [138, 139]. In their studies, they suggested that the hydrogen bonds between the monomers possess a significant aromaticity . The hydrogen bonds in $(HF)_3$ trimer were here reexamined; the degree of aromaticity and electron correlation were studied by applying ARCS and GIMIC methods [3].

The calculation of the magnetic shielding function along the symmetry axis (the ARCS function) illustrated in Figure 4.7 shows that the long-range magnetic shielding vanishes outside the electron charge density indicating that the molecular ring does not sustain any strong ring current. By using the GIMIC approach, the ring-current susceptibilities of 0.34 and 0.44 nA/T for the $(HF)_3$ trimer were obtained at the MP2 and B3LYP levels. The current profiles of the current passing a cut plane through the HF bond and through the hydrogen bond of the $(HF)_3$ trimer are shown in Figure 4.8. In Figure 4.9, the magnetically induced current density in the complex plane is revealed. The GIMIC calculations clearly demonstrates that the currents predominantly circles around the HF monomers rather than the entire trimer. Both ARCS and GIMIC calculations give the same conclusion that the $(HF)_3$ ring is nonaromatic. The problem in using the NICS values simply as an aromaticity index without careful consideration has been canvassed by Lazzeretti *et al.* [111], and another example is here presented.

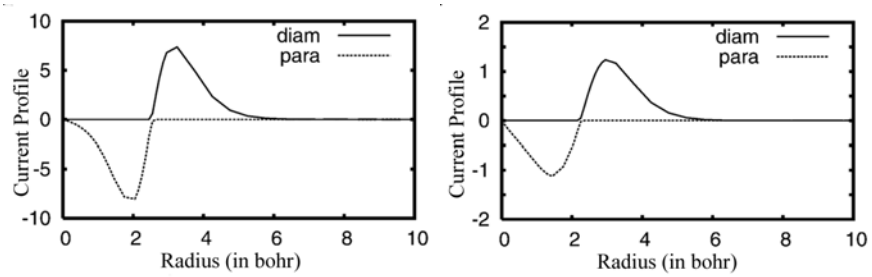

Figure 4.8: Diamagnetic and paramagnetic currents passing a cut plane (a) through the HF bond and (b) through the hydrogen bond of the $(HF)_3$ trimer. Note that the maximum for the hydrogen bond is about a factor of 6 smaller than that for the HF molecule. The calculation was performed at the MP2/ TZVPP level.

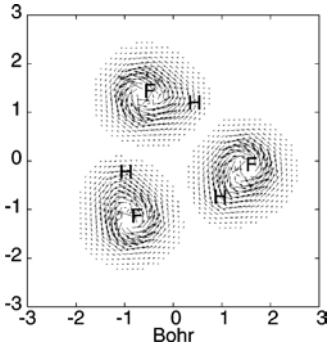

Figure 4.9: Magnetically induced current density of $(HF)_3$ in the molecular plane calculated at the MP2/TZVPP level.

Chapter 5

Summary

THE aim of the studies in the thesis is to provide the microscopic information of small bimetallic clusters in order to acquire a better understanding of mixed-metal systems. Small lithium-aluminum clusters were investigated at the CCSD level. The obtained molecular structures form four-membered Al_4^{2-} and Al_4^{4-} rings with the Li atoms acting as counterions. Many methods for assessing the degree of aromaticity have been developed. They have been successfully used to determine the aromaticity of the traditional organic compounds. This system immediately became a popular touchstone, and then the term "σ aromaticity" came along in order to describe the aromaticity contributed from σ orbitals. The M_4^{2-} (M=Cu, Ag, and Au) clusters were predicted by Wannere *et al* to have a similar structure as Al_4^{2-} [140]. In our studies, the GIMIC method was applied to the Al_4^{2-}, Al_4^{4-} and Cu_4^{2-} clusters at the CCSD level. This series of calculations showed that these rings sustain strong diatropic currents the σ orbitals. The currents induced in the π orbitals are diatropic in Al_4^{2-} and paratropic in Al_4^{4-} whereas the Cu_4^{2-} ring sustains currents mainly in the σ orbitals. Based on NICS calculations, Wannere *et al* propsed that the alkali-coinage metal clusters are the first example of *d*-orbital aromatic molecules, whereas our GIMIC calculations showed that the *d*-orbitals do not significantly participate in the current flux around the ring. In the computational $(HF)_3$ study, the obtained ring-current susceptibility is only 0.37 nA/T at the MP2 level showing that $(HF)_3$ is not an aromatic complex as suggested by Rehaman *et al* [139]. The weak diatropic and paratropic currents flowing around the complex almost cancel while the substantial edge currents of 9.1 nA/T circling around the monomers give arise to the significant magnetic shielding values at the center of the trimer.

The negatively charged $NaCu_4^-$ and sodium-auride clusters with the composition of $Na_mAu_n^-$ ($n = 1 - 4, n \geq m$ and $m + n \leq 6$) were generated and studied spectroscopically as well as computationally. Photoelectron spectroscopy has been combined with *ab initio* calculations to examine the molecular structures of the anionic clusters. A striking difference between Cu_4^{2-} and Au_4^{2-} structures was found. The copper species has a ring-shaped Cu_4^{2-} core whereas $NaAu_4^-$ is a planar cluster of C_{2v} symmetry. Because the excess electron is mainly distributed on the gold atoms, the gold atoms orient themselves away from each other. The sodium-auride clusters form planar structures analogously to small gold clusters: the small anionic clusters prefer to be linear or quasi-linear due to the Coulomb repulsion. A comprehensive strategy for interpretation of experimental photoelectron spectroscopic data has been conceived. The vertical detachment energies deduced from the *ab initio* calculations are found to have an accuracy of 0.2 eV as compared to experimental values rendering reliable identification of alkali-coinage metal clusters feasible.

Bibliography

[1] Lin, Y.-C.; Jusélius, J.; Sundholm, D.; Gauss, J. *J. Chem. Phys.* **2005**, *122*, 214308.

[2] Lin, Y.-C.; Sundholm, D.; Jusélius, J.; Cui, L. F.; Li, X.; Zhai, H. J.; Wang, L. S. *J. Phys. Chem. A* **2006**, *110*, 4244.

[3] Lin, Y.-C.; Sundholm, D. *J. Chem. Theory Comput.* **2006**, *2*, 761.

[4] Cui, L.-F.; Lin, Y.-C.; Sundholm, D.; Wang, L.-S. *J. Phys. Chem. A* **2007**, *111*, 7555.

[5] Sinfelt, J. H. *Bimetallic Catalysts: Discoveries, Concepts, and Applications*; Wiley: New York, 1983.

[6] Zhang, C.; Yoon, B.; Landma, U. *J. Am. Chem. Soc.* **2007**, *129*, 2228.

[7] Grosch, G. H.; Range, K.-J. *J. Alloys Compd.* **1996**, *233*, 30.

[8] Koenig, C.; Christensen, N. E.; Kollar, J. *Phys. Rev. B* **1983**, *29*, 6481.

[9] Christensen, N. E.; Kollar, J. *Solid State Commun.* **1983**, *46*, 727.

[10] Watson, R. E.; Weinert, M. *Phys. Rev. B* **1993**, *49*, 7148.

[11] Pyykkö, P. *Angew. Chem. Int. Ed.* **2002**, *41*, 3573.

[12] Pelton, A. D. *Bull. Alloy Phase Diagrams* **1986**, *7*, 136.

[13] Gabral, B. J. C.; Fernandes, F. M. S. S. *AIP Conf. Proc.* **1995**, *330*, 129.

[14] Matsunaga, S. J. *Phys. Soc. Jpn.* **2000**, *69*, 1712.

[15] Stangassinger, A.; Knight, A. M.; Duncan, M. A. *J. Phys. Chem. A* **1999**, *103*, 1547.

[16] Neubert, A.; Zmbov, K. F. *Trans. Faraday Soc.* **1974**, *70*, 2219.

[17] Piacente, V.; Gingerich, K. A. *High Temp. Sci.* **1977**, *9*, 189.

[18] Busse, B.; Weil, K. G. *Angew. Chem., Int. Ed. Engl.* **1979**, *18*, 629.

[19] Busse, B.; Weil, K. G. *Ber. Bunsen-Ges. Phys. Chem.* **1981**, *85*, 309.

[20] Scheuring, T.; Weil, K. G. *Int. J. Mass. Spectrom. Ion Phys.* **1983**, *47*, 227.

[21] Balducci, G.; Ciccioli, A.; Gigli, G. *J. Chem. Phys.* **2004**, *121*, 7748.

[22] Cui, L. F.; Li, X.; Wang, L. S.; Lin, Y. C.; Sundholm, D. *J. Phys. Chem. A* **2007**, (to be published).

[23] Hückel, E. *Z. Phys.* **1931**, *70*, 204.

[24] Pauling, L.; Sherman, J. *J. Chem. Phys.* **606**, *1*, 1933.

[25] Hehre, W. J.; McIver, R. T.; Pople, J. A.; v. R. Schleyer, P. *J. Am. Chem. Soc.* **1974**, *96*, 7162.

[26] Schleyer, P. v. R.; Maerker, C.; Dransfeld, A.; Jiao, H.; van Eikema Hommes, N. J. R. J. *J. Am. Chem. Soc.* **1996**, *118*, 6317.

[27] Pauling, L. *J. Chem. Phys.* **1936**, *4*, 673.

[28] London, F. *J. Phys. Radium* **1937**, *8*, 397.

[29] Lonsdale, K. *Proc. R. Soc. (London) A* **1937**, *159*, 149.

[30] Dauben, H. J.; Wilson, J. D.; Laity, J. L. *J. Am. Chem. Soc.* **1968**, *90*, 811.

[31] Krygowski, T. M.; Cyrański, M. *Tetrahedron* **1996**, *52*, 1713.

[32] Lazzeretti, P. *Prog. in Nucl. Magn. Res. Spect.* **2000**, *36*, 1.

[33] Gomes, J. A. N. F.; Mallion, R. B. *Chem. Rev.* **2001**, *101*, 1349.

[34] Ligabue, A.; Soncini, A.; Lazzeretti, J., P. *Am. Chem. Soc.* **124**, *124*, 2008.

[35] Heisenberg, W. *Zeitschrift für Physik* **1927**, *43*, 172.

[36] Schrödinger, E. *Phys. Rev.* **1926**, *28*, 1049.

[37] Dirac, P. A. M. *Proc. R. Soc. A* **1928**, *117*, 610.

[38] Dirac, P. A. M. *Proc. Royal Soc. A (London)* **1929**, *123*, 714.

[39] Parr, R. G.; Yang, W. *Density Functional Theory of Atoms and Molecules*; Oxford University Press: New York, 1989.

[40] Born, M.; Oppenheimer, R. *Ann. Phys.* **1927**, *84*, 457.

[41] Helgaker, T.; Jørgersen, P.; Olsen, J. *Molecular Electronic-Structure Theory*; Wiley: Chichester, 2000.

[42] Taylor, P. R. Coupled-Cluster Methods in Quantum Chemistry. In *European Summer School in Quantum Chemistry*; Roos, B. O., Widmark, P.-O., Eds.; Lund Universitet, 2005; Vol. 2, p 359.

[43] Siegbahn, P. E. M. The Configuration Interaction Method. In *European Summer School in Quantum Chemistry*; Roos, B. O., Widmark, P.-O., Eds.; Lund Universitet, 2005; Vol. 1, p 243.

[44] Almlöf, J.; Ahlrichs, R. Notes on Hartree-Fock Theory and Related Topics. In *European Summer School in Quantum Chemistry*; Roos, B. O., Widmark, P.-O., Eds.; Lund Universitet, 2005; Vol. 1, pp 171–240.

[45] Levine, I. *Quantum Chemistry*, 5th ed.; Prentice-Hall, 2000.

[46] Szabo, A.; Ostlund, N. S. *Modern Quantum Chemistry*; Dover, 1996.

[47] Atkins, P. W.; Friedman, R. S. *Molecular Quantum Mechanics*, 4th ed.; Oxford University Press, 2005.

[48] Jusélius, J. *Theoretical investigation of magnetically induced currents in closed-shell molecules*; Ph.D. Thesis, Department of Chemistry, University of Helsinki, 2004.

[49] Lehtonen, O. *Quantum chemical studies of supramolecular complexes and nanoclusters*; Ph.D. Thesis, Department of Engineering Physics and Mathematics, Helsinki University of Technology, 2007.

[50] Blinder, S. M. *Am. J. Phys.* **1965**, *33*, 431.

[51] Roothaan, C. C. J. *Rev. Mod. Phys.* **1951**, *23*, 69.

[52] Hall, G. G. *Proc. R. Soc. (London)* **1951**, *A205*, 541.

[53] Pulay, P. *Chem. Phys. Lett.* **1980**, *73*, 393.

[54] Pulay, P. *J. Comp. Chem.* **1982**, *3*, 556.

[55] Nunes, R. W.; Vanderbilt, D. *Phys. Rev.* **1994**, *B50*, 17611.

[56] Li, X.-P.; Nunes, R. W.; Vanderbilt, D. *Phys Rev.* **1993**, *B47*, 10891.

[57] Ochsenfeld, C.; Head-Gordon, M. *Chem. Phys. Lett.* **1997**, *270*, 399.

[58] Strout, D. L.; Scuseria, G. E. *J. Chem. Phys.* **1995**, *102*, 8448.

[59] Strain, M. C.; Scuseria, G. E.; Frisch, M. J. *Science* **1996**, *271*, 51.

[60] Milla, J. M.; Scuseria, G. E. *J. Chem. Phys.* **1997**, *106*, 5569.

[61] Lödwin, P. O. *Rev. Mod. Phys.* **1962**, *34*, 80.

[62] Crawford, T.; Schaefer, H. *An introduction to coupled-cluster theory for computaitonal chemists*; 2000.

[63] Koch, H.; Christiansen, O.; Olsen, J. *Chem. Phys. Lett.* **1995**, *244*, 75.

[64] Christiansen, O.; Koch, H.; Jørgensen, P.; Olsen, J. *Chem. Phys. Lett* **1996**, *256*, 185.

[65] Christiansen, O.; Koch, H.; Jørgensen, P. *Chem. Phys. Lett.* **1995**, *243*, 409.

[66] Raghavachari, K.; Trucks, G. W.; Pople, J. A.; Head-Gordon, M. *Chem. Phys. Lett.* **1989**, *157*, 479.

[67] Urban, M.; Noga, J.; Cole, S. J.; Bartlett, R. J. *J. Chem. Phys* **1985**, *83*, 4041.

[68] Helgaker, T.; Jørgensen, *Theor. Chim. Acta* **1989**, *75*, 111.

[69] Koch, H. J. A. J. P., H. Jensen; Helgaker, T.; Scuseria, G. E.; Schaefer III, H. F. *J. Chem. Phys.* **1990**, *92*, 4924.

[70] Stanton, J. F.; Bartlett, R. J. *J. Chem. Phys.* **1993**, *98*, 7029.

[71] Feyereisen, M.; Fitzgerald, G.; Komornicki, A. *Chem. Phys. Lett.* **1993**, *208*, 359.

[72] Christiansen, O.; Koch, H.; Jørgensen, P. *Chem. Phys. Lett.* **1995**, *243*, 409.

[73] Christiansen, O.; Koch, H.; Jørgensen, P. *J. Chem. Phys.* **1995**, *103*, 7429.

[74] Møller, C.; Plesset, M. S. *Phys. Rev.* **1934**, *46*, 618.

[75] Roos, B. O.; Taylor, P. R.; Siegbahn, P. E. M. *Chem. Phys.* **1980**, *48*, 157.

[76] Hohenberg, P.; Kohn, W. *Phys. Rev. B* **1964**, *136*, 864.

[77] Kohn, W.; Sham, L. J. *Phys. Rev. A* **1965**, *140*, 1133–1138.

[78] Handy, N. C. Density Functional Theory. In *European Summer School in Quantum Chemistry*; Roos, B. O., Widmark, P.-O., Eds.; Lund Universitet, 2005; Vol. 2, pp 401–542.

[79] Helgaker, T. Analytical Gradient Theory. In *European Summer School in Quantum Chemistry*; Roos, B. O., Widmark, P.-O., Eds.; Lund Universitet, 2005; Vol. 2, pp 429–465.

[80] Ruud, K. *Magnetic properties of closed-shell molecules*; Ph.D. Thesis, Department of Chemistry, University of Oslo, 1998.

[81] Koch, H.; Christiansen, O.; Jørgensen, P.; de Merás, A. M. S.; Helgaker, T. *J. Chem. Phys.* **1997**, *106*, 1808.

[82] Epstein, S. T. *J. Chem. Phys.* **1973**, *58*, 1592.

[83] Davis, D. W. *The Theory of the Electric and Magnetic Properties of Molecules*; John Wiley and Sons, 1967.

[84] Pedersen, T. B.; Koch, H. *J. Chem. Phys.* **1997**, *106*, 8059.

[85] London, F. *J. Phys. Radium* **1937**, *8*, 397.

[86] Gauss, J.; Ruud, K.; Helgaker, T. *J. Chem. Phys.* **1996**, *105*, 2804.

[87] Pulay, P. In *Modern Electronic Structure Theory*; Yarkony, D. R., Ed.; World Scientific: Singapore, 1995; Vol. 2, p 1191.

[88] Chen, Z.; Wannere, C. S.; Corminboeuf, C.; Puchta, R.; v. R. Schleyer, P. *Chem. Rev.* **2005**, *105*, 3842.

[89] Hoarau, J. *Ann. Chim. (Paris)* **1956**, *1*, 527.

[90] Dauben, H. J.; Wilson, J. D.; Laity, J. L. *J. Am. Chem. Soc.* **1969**, *91*, 1991.

[91] Dauben Jr, H. J.; Wilson, J. D.; Laity, J. L. *Non-benzenoid Aromatics*; Academic Press: New York, 1971; Vol. 2.

[92] Luyten, P. R.; Bulthuis, J.; Maclean, C. *Chem. Phys. Lett.* **1982**, *89*, 287.

[93] Sutter, D. H.; Flygare, W. H. *J. Am. Chem. Soc.* **1969**, *91*, 4063.

[94] Flygare, W. H.; Benson, R. C. *Mol. Phys.* **1971**, *20*, 225.

[95] Flygare, W. H. *Chem. Rev.* **1974**, *74*, 653.

[96] Günther, H. *NMR Spectroscopy: Basic Principles, Concepts, and Applications in Chemistry*, 2nd ed.; Wiley and Sons, 1995.

[97] Lazzeretti, P. *Prog. Nucl. Magn. Res. Spectr.* **2000**, *36*, 1.

[98] Schreckenbach, G.; Ziegler, T. *Theor. Chem. Acc.* **1998**, *99*, 71.

[99] Bühl, M.; Kaupp, M.; Malkina, O. L.; Malkin, V. *J. Comput. Chem.* **1999**, *99*, 71.

[100] Wang, B.; Fleischer, U.; Hinton, P. J. F.; Pulay, P. J. *Comput. Chem.* **2001**, *22*, 1887.

[101] Günther, H. *NMR Spectroscopy: Basic Principles, Concepts, and Applications in Chemistry*, 2nd ed.; John Wiley & Sons, 1995.

[102] Mitchell, R. H. *Chem. Rev.* **2001**, *101*, 1301.

[103] Schleyer, P. v. R.; Manoharan, M.; Wang, Z. X.; Kiran, B.; Jiao, H.; Puchta, R.; Hommes, N. J. R. V. E. *Org. Lett.* **2001**, *3*, 2465.

[104] Nyulaszi, L.; Schleyer, P. v. R. *Am. Chem. Soc.* **1999**, *121*, 6872.

[105] Alkorta, I.; Elguero, J. *J. New J. Chem* **1999**, *23*, 951.

[106] Krygowski, T. M.; Cyrański, M. K. *Chem. Rev.* **2001**, *101*, 1385.

[107] Cyrański, M. K.; K., T. M.; Katritzky, A. R.; Schleyer, P. v. R. *Org. Chem.* **2002**, *67*, 1333.

[108] Jusélius, J.; Straka, M.; Sundholm, D. *J. Phys. Chem. A* **2001**, *105*, 9939.

[109] Jusélius, J.; Patzschke, M.; Sundholm, D. *J. Mol. Struct. (Theochem)* **2003**, *633*, 123.

[110] Aihara, J. *Chem. Phys. Letters* **2002**, *365*, 34.

[111] Lazzeretti, P. *Phys. Chem. Chem. Phys.* **2004**, *6*, 217.

[112] Jusélius, J.; Sundholm, D. *Phys. Chem. Chem. Phys.* **1999**, *1*, 3429.

[113] Arfken, G. *Mathematical Methods for Physicists*; Academic Press: Orlando, 1985.

[114] Jusélius, J.; Sundholm, D.; Gauss, J. *J. Chem. Phys.* **2004**, *121*, 3952.

[115] Lonsdale, K. *Proc. R. Soc. (London) A* **1937**, *159*, 149.

[116] London, F. *C.R. Acad. Sci.* **1937**, *205*, 159.

[117] Pople, J. A. *J. Chem. Phys.* **1956**, *24*, 1111.

[118] Pople, J. A. *Mol. Phys.* **1958**, *1*, 175.

[119] McWeeny, R. *Mol. Phys.* **1958**, *1*, 311.

[120] Jusélius, J.; Sundholm, D.; Gauss, J. *J. Chem. Phys.* **2004**, *121*, 3952.

[121] Li, X.; Kuznetsov, A. E.; Zhang, H. F.; Boldyrev, A. I.; Wang, L. S. *Science* **2001**, *291*, 859.

[122] Kuznetsov, A. E.; Birch, K. A.; Boldyrev, A. I.; Li, X.; Zhai, H. J.; Wang, L. S. *Science* **2003**, *300*, 622.

[123] Chen, Z.; Corminboeuf, C.; Heine, T.; Bohmann, J.; v. R. Schleyer, P. *J. Am. Chem. Soc.* **2003**, *125*, 13930.

[124] Tsipis, A. C.; Tsipis, C. A. *J. Am. Chem. Soc.* **2003**, *125*, 1136.

[125] Tsipis, A. C.; Karagiannis, E. E.; Kladou, P. F.; Tsipis, C. A. *J. Am. Chem. Soc.* **2004**, *126*, 12916.

[126] Fuentealba, P.; Padilla-Campos, L. *Intern. J. Quantum Chem.* **2005**, *102*, 498.

[127] Hoshino, K.; Naganuma, T.; Watanabe, K.; Nakajima, A.; Kaya, K. *Chem. Phys. Lett.* **1993**, *211*, 571.

[128] Heiz, U.; Vayloyan, A.; Schumacher, E.; Yeretzian, C.; Stener, M.; Gisdakis, P.; Rösch, N. *J. Chem. Phys.* **1996**, *105*, 5574.

[129] Heiz, U.; Vayloyan, A.; Schumacher, E. *J. Phys. Chem.* **1996**, *100*, 15033.

[130] Baruah, T.; Blundell, S. A.; Zope, R. R. *Phys. Rev. A* **2001**, *64*, 043202.

[131] Moran, D.; Simmonett, A. C.; Leach III, F. E.; Allen, W. D.; Schleyer, S. I. H. F., P. v. R. *J. Am. Chem Soc.* **2006**, *128*, 9342.

[132] Wang, L. S.; Cheng, H. S.; Fan, J. *J. Chem. Phys.* **1995**, *102*, 9480.

[133] Johansson, M. P.; Jusélius, J.; Sundholm, D. *Angew. Chem. Int. Ed.* **2005**, *44*, 1843.

[134] Chen, Z.; Heine, T.; Sundholm, D.; von Ragué Schleyer, P. Aromaticity Indices from Magnetic Shieldings. In *Quantum Chemical Calculation of Magnetic Resonance Properties*; Kaupp, M., Bühl, M., Malkin, V., Eds.; Wiley-VCH: Weinheim, Germany, 2004; pp 395–407.

[135] Gauss, J. *J. Chem. Phys.* **1993**, *99*, 3629.

[136] Steiner, E.; Fowler, P. W. *Phys. Chem. Chem. Phys.* **2004**, *6*, 261.

[137] Bergman, D. L.; Laaksonen, L.; Laaksonen, A. *J. Mol. Graphics & Modelling* **1997**, *15*, 301.

[138] Datta, A.; Pati, S. K. *Intern. J. Quant. Chem.* **2006**, *106*, 1697.

[139] Rehaman, A.; Datta, A.; Mallajosyula, S. S.; Pati, S. K. *J. Chem. Theory Comput.* **2006**, *2*, 30.

[140] Wannere, C. S.; Corminboeuf, C.; Wang, Z. X.; Wodrich, M. D.; King, R. B.; v R Schleyer, P. *J. Am. Chem. Soc.* **2005**, *127*, 5701.